DOKUZ EYLÜL UNIVERSITY

GRADUATE SCHOOL OF NATURAL AND APPLIED SCIENCES

FAILURE ANALYSIS OF PIN-LOADED COMPOSITE PLATES

by

Özgür AHISHALI

February, 2006

İZMİR

FAILURE ANALYSIS OF PIN-LOADED COMPOSITE PLATES

A Thesis Submitted to the
Graduate School of Natural and Applied Sciences of Dokuz Eylül University
In Partial Fulfillment of the Requirements for the Degree of Master of Science
in Mechanical Engineering, Mechanics Program

by
Özgür AHISHALI

February, 2006
İZMİR

Ms. Sc. THESIS EXAMINATION RESULT FORM

We have read the thesis, entitled **"FAILURE ANALYSIS OF PIN-LOADED COMPOSITE PLATES"** completed by **ÖZGÜR AHISHALI** under supervision of **Prof. Dr. ONUR SAYMAN** and we certify that in our opinion it is fully adequate, in scope and in quality, as a thesis for the degree of Master of Science.

Prof. Dr. Onur SAYMAN

Supervisor

(Committee Member)

(Committee Member)

Prof. Dr. Cahit Helvacı
Director
Graduate School of Natural and Applied Sciences

ACKNOWLEDGEMENT

FAILURE ANALYSIS OF PIN-LOADED COMPOSITE PLATES

ABSTRACT

The aim of this study is to search the failure load, bearing strength and failure mode in an aluminum-glass epoxy sandwich composite plate subjected by a bolt impacted by a preload and washer on a circular hole. In experiments without a preload moment, the hole of the plate exposed to a traction force by a rigid pin.

Parametric studies were performed by experiments to find the effects of joint geometry and preload moment on the failure load and failure mode. The preload moment (M), end distance to diameter (E/D) and width to diameter ratios (W/D) changed from 0-3-6 Nm, 1 to 5 and 2 to 5 sequentially. During the numerical and experimental study, orientation angle θ hold constant at 0 ^{o}. The failure analysis is performed both numerically and experimentally.

From the results of this study, it is observed that with increasing of M, E/D, W/D the bearing strength increases; and when M = 0-3-6 Nm, E/D = 2-3-4-5 and W/D = 5 full bearing mode occurs. When E/D = 1 the failure mode is always Shear-out for all parameters.

Lusas 13.6 finite element analysis program was used for numerical study. Three dimensional finite element method was taken as a base. Maximum failure load was obtained with non-linear analysis and Hashin failure criteria was used.

In the case of failure, appropriate properties of failure mode was reduced.

By the help of standard tests, composite material's mechanical properties were determined.

From the comparison of the numerical and experimental studies sensible agreement was seen between the results where full bearing mode observed.

Keywords: c. sandwich, failure strength, failure mode, preload, composite plates

PİM YÜKLÜ KOMPOZİT PLAKALARDAKİ HASAR ANALİZİ

ÖZET

Bu çalışmanın amacı, bir rondela ile ön yüklemeye maruz kalmış dairesel delik üzerindeki saplamayla ilişkilendirilmiş alüminyum-cam epoksi sandviç kompozit plakadaki hasar yükü ve hasar modunun araştırılmasıdır. Ön yüklemesiz deneylerde plakanın deliği, rijit bir pim tarafından çekme yüküne maruz kalmıştır.

Ön yükleme momenti (M), daire merkezinin plakanın sonuna uzaklığının (E/D) ve plaka genişliğinin; çapa oranları (W/D) sırasıyla; 0-3-6 Nm, 1 den 5'e kadar ve 2 den 5'e kadar değiştirilmiştir. Nümerik ve deneysel çalışmalar sırasında yönlenme açısı θ sabit olarak 0° tutulmuştur. Hasar analizi hem sayısal hemde deneysel olarak yapılmıştır.

Bu çalışmaların sonucunda hasar yükünün M, E/D, W/D oranlarının artışıyla arttığı ve M = 0-3-6 Nm, E/D = 2-3-4-5 ve W/D = 5 iken tam yatak gerilmesinin oluştuğu gözlemlenmiştir. E/D = 1 durumunda tüm parametrelerde kayma hasarının oluştuğu görülmüştür.

Nümerik çalışma için Lusas 13.6 sonlu elemanlar analiz programı kullanılmıştır. Üç boyutlu sonlu elemanlar metodu baz alınmış, Hashin hasar kriteri kullanılarak maksimum hasar yükü lineer olmayan analiz yöntemiyle belirlenmiştir.

Hasar durumunda, kompozit plağın hasarlı nodlarındaki malzeme özellikleri indirgenmiştir.

Standart testlerin yardımıyla kompozit malzemenin mekanik özellikleri belirlenmiştir.

Karşılaştırmalar sonucunda nümerik ve deneysel çalışmaların sonuçlarında hasar modu tam yatak gerilmesine yaklaştığında kabul edilebilir bir uyum görülmüştür.

Anahtar kelimeler : Kompozit sandviç, hasar yükü, hasar modu, ön yükleme, kompozit plaka

CONTENTS

NOMENCLATURE

D	Hole diameter	mm
E	End distance from the hole center	mm
W	Width of the plate	mm
t	Thickness of the plate	mm
L	Distance from hole center to fixed end	mm
a, b, c,ti	Dimensions of Iosipescu testing specimen	mm
F_{max}	Repture load applied Iosipescu testing specimen	N
P	Tensile load	N
P_{max}	Maximum failure load	N
E_1, E_2	Elastic moduli in the material directions	GPa
G_{12}	Shear modulus	GPa
υ_{12}	Poisson's ratio	-
V_f	Fiber volume fraction	%
σ_b	Bearing strength	MPa
X_t	Tensile strength in the fiber direction	MPa
X_c	Compressive strength in the fiber direction	MPa
X_y	Yield strength in the fiber direction	MPa
Y_t	Tensile strength in the transverse direction	MPa
Y_c	Compressive strength in the transverse direction	MPa
Y_y	Yield strength in the transverse direction	MPa
S	Shearing strength	MPa
ε_1	Longitudinal strain	-
ε_2	Transverse strain	-
M	Preload moment	Nm
$[C_{ij}]$	Inverse of compliance matrix	
$[S_{ij}]$	Compliance matrix	
u, v, w	Displacement component	
$[\overline{C}_{ij}]$	Reduced-stiffness matrix	

CHAPTER ONE
INTRODUCTION

Composite materials uses in structures comprehensively where high mechanical performance required and in designing ratio of high strength to weight takes care initially.

Getting high strength and stiffness values while keeping weight in the low values provides the composites to take the place of metal materials used since immemorial.

In the structures made of composite laminates mechanical fasteners has a great importance at transferring loads and for this transaction a hole should be drilled on them. This holes causes stress concentration, in spite of these negativeness mechanical fasteners has a part in aeroplane industry rather frequently.

A non-appropriate joint design, causes low yielding although composites has a high level strength; stress distribution over the hole wall should be considered straightly for sufficiently qualified strength evaluation and a realistic failure prediction.

Because of the anisotropic and heterogeneous nature of the composites joint problem analysis is plenty of harder than the isotropic materials; separately owing to the unknown contact stresses and contact area between fastener and laminate, pin-loaded hole analysis is more complicated in comparison with free hole.

In this respect; many studies were carried out about mechanical fastened joints in the composite structures and in many of these studies for getting a suitable stress analysis or failure analysis prediction, before all else experimental studies investigated.

In spite of all these disadvantages mechanical fastened joints involved in industry frequently because of their peculiarities like low cost, easy assemble and disassemble and easy mending.

Chang (1984) a carried out analysis on T300/1034-C laminates has one pin-loaded hole and two pin-loaded holes (parallel, serial), never the less Chang (1984) b have

1

developed a model and a computer code for composite laminates having a pin loaded hole to determine failure strength and failure mode , when the material exhibits non-linearly elastic behavior.

Mahmood and Larry (1995) have carried out a numerical and experimental study over the pin-loaded composites to find the three dimensional non-linear stresses.

Collings (1977) investigated the effects of geometric parameters, bolt clamping pressure and ply orientation and than carried out a study (1982) to investigate the relation between W/D, E/D, t/D and joint strength by testing CFRP for a series, laminate configuration and hole diameters.

Chen (1994) investigated the effects of reinforcement type, weave structure and geometric parameters on pin-loaded strength at three dimensional orthogonal composites.

Stockdale and Mathews (1976) studied clamping pressure's effects on the bold bearing load for glass fiber-reinforced plastics experimentally.

Godwin and Mathews (1989); Camaho and Mathews (1997) investigated the effects of geometric parameters, joint parameters and material properties on mechanical fastened joint's strengths of fiber reinforced plastics.

Hassan (1996) investigated failure analysis of single and multi-bolted double shear lap connections of glass-fiber reinforced plastics with the help of a three dimensional finite element model using ANSYS.

Pierron (2000) investigated the stress distribution at the hole of woven composite joints by using ABAQUS.

Mathews (1982) carried out an finite element analysis to point at stress distribution of the loaded hole on fiber reinforced laminates depends upon the whether the load is applied to a pin or a bolt.

Zhang and Ueng (1987) carried out a study by using a method which uses Leckhnitskii's method in the terms of displacement to find the normal and shear stresses at the hole boundary.

Dano (2000) observed the progressive failure damage of pin loaded composite plate to predict the bearing stress- pin displacement curve just before joint failure occurs.

Mathews (1979) carried out a study by compressing single and multi hole bolted joints of glass-fiber reinforced plastics to point at increasingly complexing of the joint geometry is opposite proportional to the joint strength.

Xiao and Ishikawa (2005) studied bearing strength and failure behavior in mechanically fastened joints.

Tong (2000) investigated the effect of the relative positions of the bolt and the washer on bearing failure behavior of bolted composite joints with various lateral constraints.

Commanho and Mathews (1999) developed a three dimensional finite element model using Hashin failure criteria to predict the strength and damage process of mechanical fastened joints in carbon fiber reinforced plastics and compared the results with the experimental studies.

Içten and Karakuzu (2002) initially designed the mechanical properties by the standard tests and than they carried out a study with a two dimensional finite element method using Hoffman and Hashin criteria to predict the pinned joint carbon epoxy composite plates. In order to make comparison they investigated the failure load and failure mode experimentally and numerically.

Içten et all (2002) carried out an experimental and numerical study using material configurations of woven glass fiber-epoxy composites ($[(0/90)_3]s-[(\pm 45)_3]s$) and twenty different geometries. Then investigated the mechanical behavior and damage development.

Aktaş and Karakuzu (1999) studied the failure analysis of mechanically fastened carbon fiber reinforced epoxy composite plates with arbitrary orientation, experimentally and numerically by using Tsai-Hill and fiber tensile-compressive failure criteria.

Içten and Sayman (2003) investigated the failure load and failure mode of the aluminium-glass-epoxy sandwich plates with a circular hole subjected to a traction force by a pin; experimentally using different joint geometries and fiber orientation.

In this study, failure modes and failure loads of the aluminium-glass-epoxy sandwich plates subjected to different preload moments with different geometries investigated initially experimentally and then numerically using ANSYS 13.6 finite element program than the results compared.

CHAPTER TWO
INTRODUCTION TO COMPOSITE MATERIALS

2.1 Characteristics of a composite material

The constituents of a composite are generally arranged so that one or more discontinuous phases are embedded in a continuous phase. The discontinuous phase is the reinforcement and the continuous phase is the matrix (Staab G. H. 1992). An exception to this is rubber particles suspended in a rigid rubber matrix, which produces a class of materials known as rubber-modified polymers. In general the reinforcements are much stronger and stiffer than the matrix. Both constituents are required, and each must accomplish specific tasks if the composite is to perform as intended.

A material is generally stronger and stiffer in fiber form than in bulk form. The number of microscopic flaws that act as fracture initiation sites in bulk materials are reduced when the material is drawn into a thinner section. In fiber form the material will typically contain very few microscopic flaws from which cracks may initiate to produce catastrophic failure. Therefore, the strength of the fiber is greater than the that of the bulk material. Without a binder material to separate them, they can become knotted, twisted, and hard to separate. The binder (matrix) material must be continuous and surround each fiber so that they are kept distinctly separate from adjacent fibers and the entire material system is easier to handle and work with.

The physical and mechanical properties of composites are depend on the properties, geometry, and concentration of the constituents. Increasing the volume content of reinforcements can increase the strength and stiffness of a composite to a point. If the volume content of reinforcements is too high there will not be enough matrix to keep them separate, and they can become tangled. Similarly, the geometry of individual reinforcements and their arrangement within the matrix can affect designing with composite materials. The type of reinforcement and matrix, the

geometric arrangement and volume fraction of each constituent, the anticipated mechanical loads, the operating environment for the composite and so forth must all be taken into account.

Analysis of composites subjected to various mechanical, thermal, and hygral conditions is the main thrust of this text. Discussions are limited to continuous fiber laminated composites. In introductory strength of materials, the constitutive relationship between stress and strain was established for homogeneous isotropic materials as Hooke's law. A composite material is analyzed in a similar manner, by establishing a constitutive relationship between stress and strain.

Isotropic, homogeneous materials (steel, aluminum, etc.) are assumed to be uniform throughout and to have the same elastic properties in all directions. Upon application of a uniaxial tensile load, an isotropic material deforms in a manner similar to that indicated in Fig.2.1. In this figures undeformed specimen showed with dashed lines. Assuming a unit width and thickness for the specimen, the transverse in-plane and out-of-plane displacements are the same. Unlike conventional engineering materials, a composite material is generally nonhomogeneous and does not behave as an isotropic material. Most composites behave as either anisotropic or orthotropic materials.
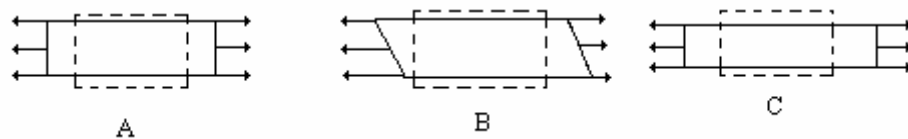
Figure.2.1. Isotropic (A), anisotropic (B), and orthotropic (C) materials responses subjected to axial tension

The material properties of an anisotropic material are different in all directions. There is typically a coupling of extension and shear deformation under conditions of uniaxial tension. The response of an anisotropic material subjected to uniaxial tension is also shown in Fig.2.1. There are varying degrees of anisotropic material

behavior, and the actual deformation resulting from applied loads depends on the material.

The material properties of an orthotropic material are different in three mutually perpendicular planes, but there is generally no shear-extension coupling as with an anisotropic material. The transverse in-plane and out-of-plane displacements are not typically the same, because Poisson's ratio is different in these two directions. Fig 2.1. shows orthotropic material response too. Although it appears similar to that of an isotropic material, the magnitudes of the in-plane and out-of –plane displacements are different.

2.2 Composite materials classification

Composite materials are usually classified according to the type of reinforcement used. Fibrous and particulate are Two broad classes of composites. Each has unique properties and application potential, their specific categories are revealed bellow.

Fibrous **:** A fibrous composite consists of either continuous (long) or chopped (whiskers) fibers suspended in a matrix material. From a geometric viewpoint Both continuous fibers and whiskers can be identified:

Continuous fibers **:** A continuous fiber is geometrically characterized as having a very high length-to-diameter ratio. They are on the whole stronger and stiffer than bulk material. Depending upon the fiber, fiber diameters arrange between 3 and 200μm in general (Watt, W., and B. V. Perov. 1985.)

Whiskers **:** A whisker is generally considered to be a short, stubby fiber. It can be broadly defined as having a length-to-diameter ratio of 5< l/d<1000 and beyond (Evans, C. C. 1972). Whisker diameters generally arrange between 0.02 and 100 μm.

Composite in which the reinforcements are discontinuous fibers or whiskers can be produced so that the reinforcements have either random or biased orientation.

Material systems consists of discontinuous reinforcements are called as single layer composites. The discontinuities can produce a material response that is anisotropic, but in many instances the random reinforcements produce nearly isotropic composites. Continuous fiber composites can be either single layer or multilayered. The single layer continuous fiber composites can be either unidirectional or woven, and multilayered composites are generally referred to as laminates. The material response of a continuous fiber composite is generally orthotropic. Schematics of both types of fibrous composites are shown in Fig.2. 2.
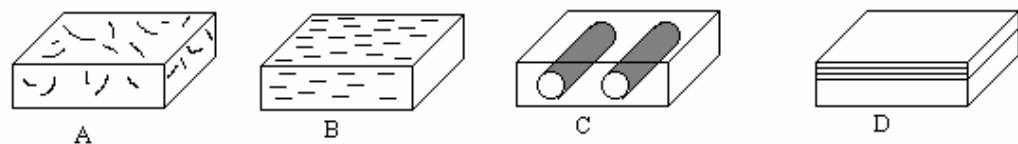
Figure.2.2. Schematic representation of fibrous composites; A : random fiber orientation; B : biased   fiber orientation (discontinuous fiber composites); C : unidirectional; D : laminated (continuous   fiber composites)

Particulate **:** A particulate composite is characterized as being composed of particles suspended in a matrix. Particles can have in a little while any size, configuration or shape. Well known Examples of particulate composites are concrete and particle board. There are two subclasses of particulates.

Flake : A flake composite is generally composed of flakes with large ratios of platform area to thickness, suspended in a matrix material.

Filled/skeletal : A filled/skeletal composite is composed of a continuous skeletal matrix filled by a second material.

The response of a particulate composite can be either anisotropic or orthotropic. Such composites are used for many applications in which strength is not a significant element for designing. Particulate composites are given in Figure.2.3.
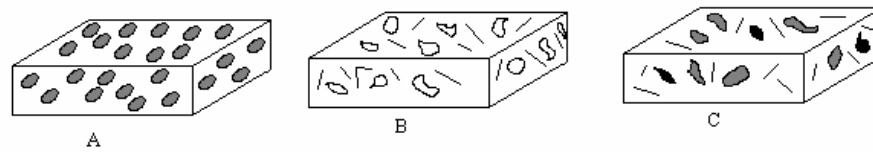
Figure.2.3. Schematic representation of particulate composites; A : general particulate; B : flake C : filled/skeletal

2.3 Composite material terminology

Lamina : A lamina is a flat or a curved arrangement of unidirectional or woven fibers suspended in a matrix material. A lamina is generally assumed to be orthotropic, and the material from which it is made designate it's thickness. For example, a graphite/epoxy lamina may be on the order of 0,127mm thick. For the purpose of analysis, a lamina is typically modeled as having one layer of fibers through the thickness. This is only a model and not a true representation of fiber arrangement. Unidirectional and woven lamina are schematically shown in Fig.2. 4.
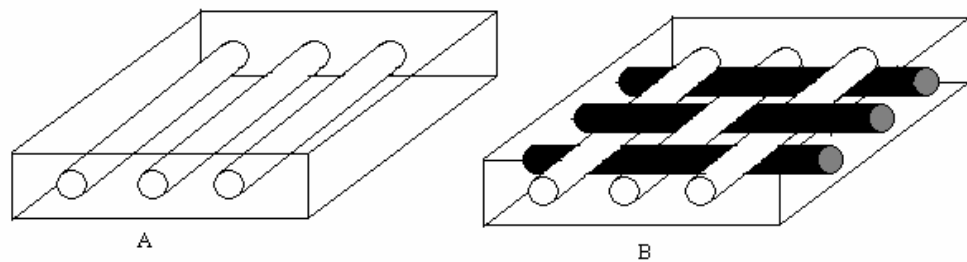
Figure. 2. 4. Schematic representation of unidirectional and woven composite lamina; A :Unidirectional; B: Woven

Reinforcements : Reinforcements are used to make the composite structure stronger. The most commonly used reinforcements are boron, glass, graphite, kevlar, aluminum, silicon carbide, silicon nitride and titanium

Fibers : Fibers are a special case of reinforcements. They are generally continuous and have diameters ranging from 3 to 200 μm. Fibers are typically linear elastic or elastic-perfectly plastic and are generally stronger and stiffer than the same material in bulk form. The most commonly used fibers are boron, glass, carbon and kevlar.

Matrix : The matrix is the binder material that supports, separates, and protects the fibers. It provides path by which load is both transferred to the fibers and redistributed among the fibers in the event of fiber breakage. The matrix typically has a lower density, stiffness, and strength than the fibers. Matrices can be brittle, ductile, elastic, or plastic. They can have either linear or nonlinear stress-strain behavior. In addition, the matrix material must be capable of being forced around the reinforcement during some stage in the manufacture of the composite. Fibers must often be chemically treated to ensure proper adhesion to the matrix. The most commonly used matrices are carbon, ceramic, metal, and polymeric. Each has special appeal and usefulness, as well as limitations and given below (Richardson, T. 1987).

Carbon matrix : A carbon matrix has a high heat capacity per unit weight. They have been used as rocket nozzles, ablative shields for reentry vehicles, and clutch and brake pads for aircraft.

Ceramic matrix : A ceramic matrix is usually brittle. Carbon, ceramic, metal, and glass fibers are typically used with ceramic matrices in areas where extreme environments are anticipated.

Glass matrix : Glass and glass-ceramic composites usually have an elastic modulus much lower than that of the reinforcement. Carbon and metal oxide fibers are the most common reinforcements with glass matrix composites. The best characteristics of glass or ceramic matrix composites is their strength at high service temperatures. The primary applications of glass matrix composites are for heat-resistant parts in engines, exhaust systems, and electrical components.

Metal matrix : A metal is especially good for high-temperature use in oxidizing environments. The most commonly used metals are iron, nickel, tungsten, titanium, magnesium, and aluminum. There are three classes of metal matrix composites.

Class 1. The reinforcement and matrix are insoluble. Reinforcement/matrix combinations in this class include tungsten or alumina/copper, BN-coated B or boron/aluminum, and boron/magnesium.

Class 2 . The reinforcement/matrix exhibit some solubility and the interaction will alter the physical properties of the composite. Reinforcement/matrix combinations included in this class are carbon or tungsten/nickel, tungsten/columbium, and tungsten/copper.

Class 3. The most critical situations in terms of matrix and reinforcement are in this class. The problems encountered here are generally of a manufacturing nature and can be solved through processing controls. Within this classes the reinforcement/matrix combinations include alumina or boron or silicon carbide/titanium, carbon or slica/aluminum, and tungsten/copper.

Polymer matrix : Polymeric matrices are the most common and least expensive. They are found in nature as amber, pitch, and resin. Some of the earliest composites were layers of fiber, cloth, and pitch. Polymers are easy to process, offer good adhesion. They are a low-density material. Because low processing temperatures, many organic reinforcements can be used. A typical polymeric matrix is either viscoelastic or viscoplastic, meaning it is affected by time, temperature, and moisture. The terms thermoset and thermoplastic are often used to identify a special property of many polymeric matrices.

Thermoset : A thermoset matrix has highly cross-linked polymer chains. After it has been processed A thermoset can not be remolded. Thermoset matrices are sometimes used at higher temperatures for composite applications.

Thermoplastic : A thermoplastic matrix has polymer chains that are not cross-linked. Although the chains can be in contact, they are not linked to each other. A thermoplastic can be remolded to a new shape when it is heated to approximately the same temperature at which it was formed.

Laminate : A lamina is made of two or more unidirectional laminae or plies stacked together at various orientations Fig.2. 5. The laminae can be of various thickness and consist of different materials (Daniel. I.M, Ishai, O. 1994). Since the principal material axes differ from ply to ply, it is more convenient to analyze laminates using a common fixed system of coordinates. The orientation of a given ply is given by the angle between the references x- axis and the major principal material axis (fiber orientation) of the ply, measured in a counterclockwise direction x-y plane.
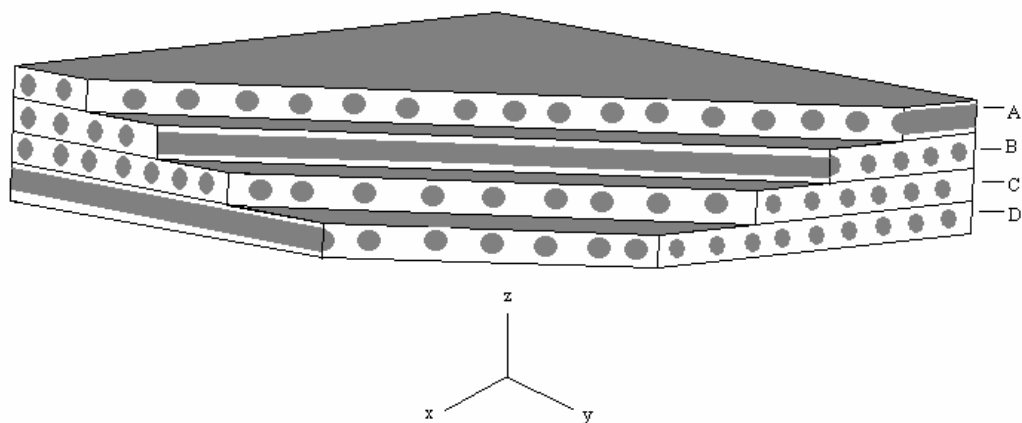
Figure. .2. 5 Multidirectional laminate and reference coordinate system; A = 0^0; B = -θ^0; C = + θ^0, D = 90^0

Composite laminates containing plies of two or more different types of materials are called hybrid composites and more specifially interply hybrid composites. For example, a composite laminate may be made up of unidirectional glass/epoxy, carbon/epoxy and aramid/epoxy layers stacked together in a specified sequence. In some cases it may be advantageous to intermingle different types of fibers, such as glass and carbon or aramid and carbon, within the same unidirectional ply. These

composites are intraply hybrid composites. One could combine intraply hybrid layer with other layers to form an intraply-interply hybrid composite.

Composite laminates are designated in a manner indicating the number, type, orientation and stacking sequence of the plies. Lay-up is the configuration of the laminate indicating it's ply composite. The configuration indicating, in addition to the ply composition, the exact location or sequence of the various plies is called the stacking sequence. Composite designations given below in Table.2. 1.

Table. 2.1. Laminate designations; S = Symmetric sequence; T = Total number of plies; ——— = Laminate is symmetric about the midplane of the ply; Number subscript = Multiple of plies; K = Kevlar; C = Carbon; G = Glass fibers

Unidirectional 6-ply	$[0/0/0/0/0/0] = [0_6]$
Crossply	$[0/90/90/0] = [0/90]_s$ $[0/90/\overline{0}] = [0/90]_s$
Angle-ply symmetric	$[+45/-45/-45-45] = [+-45]_s$ $[30/-30/30/-30/-30/30/-30/30] = [+-30]_{2s}$
Angle-ply asymmetric	$[30/-30/30/-30/30/-30/30/-30] = [+-30]_4$
Multi directional	$[0/45/-45/-45/45/0] = [/+-45]_s$ $[0/0/45/-45/0/0/0/0/-45/45/0/0] = [0_2/+-45/0_2]_s$ $[0/15/-15/15/-15/0] = [0/+-15/+-15/0]_T = [0/(+-15)_2/0]_T$
hybrid	$[0^K/0^K/45^C/-45^C/90^G/-45^C/45^C/0^K/0^K]_T = [0^K_2/+-45^C/\overline{90^G}]_s$

2.4 Micromechanics and Macromechanics

Composite materials can be viewed and analyzed at different levels and on different scales, depending on the particular characteristics and behavior under consideration. A schematic diagram of the various levels of consideration and the corresponding types of analysis is given in Figure.2.6.
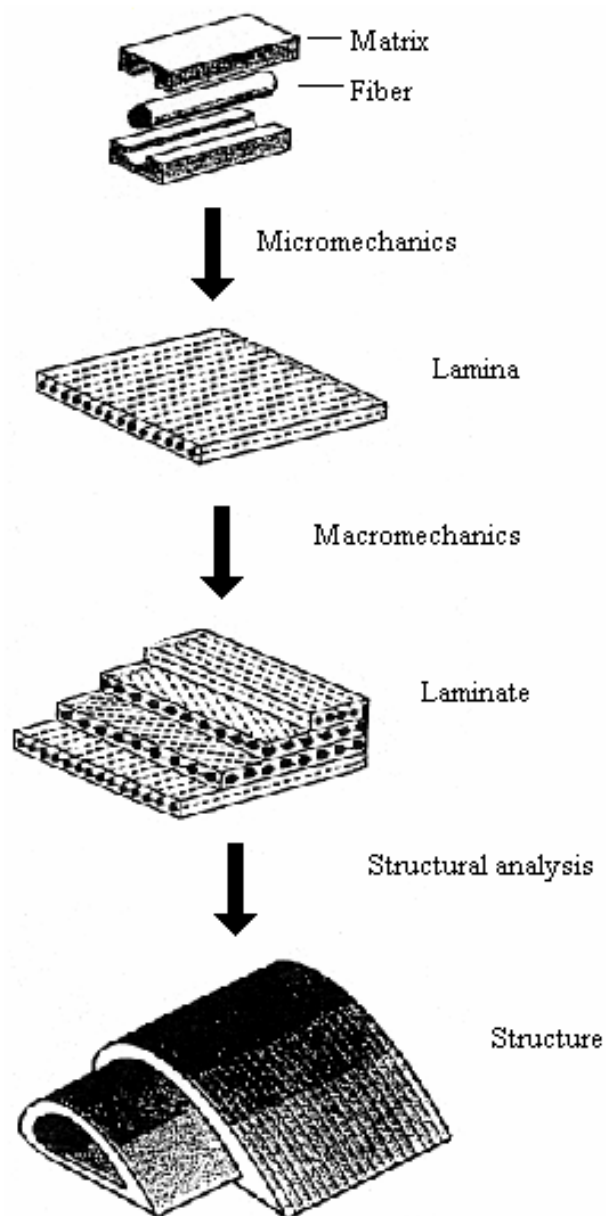
Figure.2. 6. Levels of observation and types of analysis for composite materials.

At the constituent level the scale of observation is on the border of the fiber diameter, particle size or matrix interstices between reinforcement. Micromechanics is the study of the interactions of the constituents on this microscopic level. It deals with the state of deformation and stress in the constituents and local failures such as

matrix failure (tensile, compressive, shear), fiber failure (tensile, buckling, splitting) and interface/interphase failure. An example of the complex stress distributions on the transverse cross section of a transversely loaded unidirectional composite is given in Fig.2. 7.
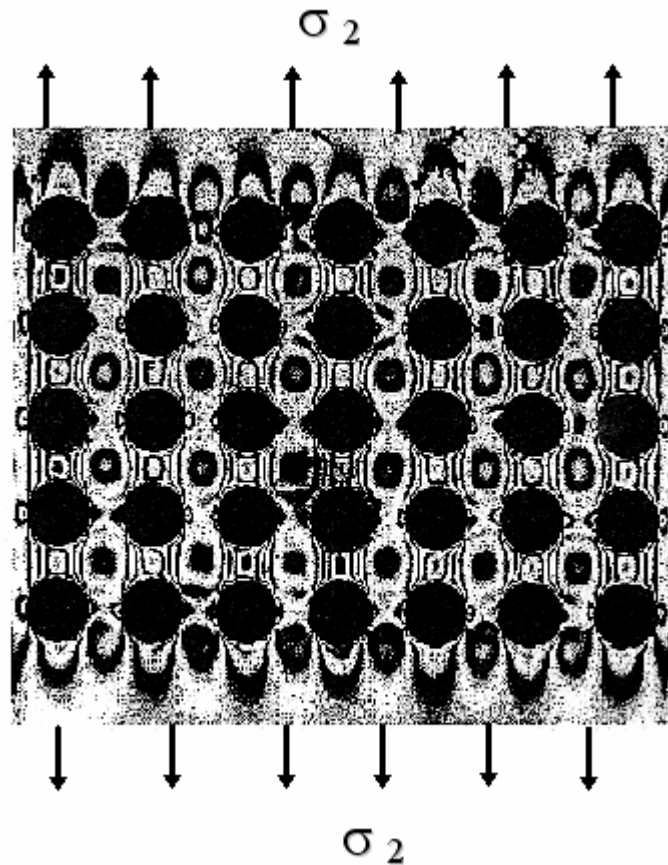
Figure.2. 7 . Isochromatic fringle patterns in a model of
transversely loaded unidirectional composite

Micromechanics is particularly important in the study of properties such as strength, fracture toughness, and fatigue life, which are strongly influenced by local characteristics that can not be integrated or averaged. Micromechanics also allows the prediction of average behavior at the lamina level as a function of constituent properties and local conditions.

At the lamina level it usually more expeditious to consider the material homogeneous, albeit anisotropic and use average properties in the analysis. This type of analysis is called macromechanics and considers the unidirectional lamina as a

quasi homogeneous anisotropic material with it's own average stiffness and strength properties. Failure criteria may be expressed in terms of average stresses and overall lamina strengths without reference to any particular local failure mechanisms. This approach is recommended in the study of the overall elastic or viscoelastic behavior of composite laminates or structures which assumes material continuity.

At the laminate level the macromechanical analysis is applied in the form of lamination theory dealing with overall behavior as a function of lamina properties and stacking sequence. At the component or structure level, methods such as finite element analysis coupled with lamination theory give the overall behavior of the structure as well as the state of stress in each lamina.

CHAPTER THREE

MACROMECHANICAL BEHAVIOR
OF AN ORTHOTROPIC LAMINA

3.1 Stress-Strain Relations in an Orthotropic Material

In an orthotropic material, three dimensional strain-stress relations can be written as:

$$\begin{Bmatrix} \varepsilon_1 \\ \varepsilon_2 \\ \varepsilon_3 \\ \gamma_{23} \\ \gamma_{31} \\ \gamma_{12} \end{Bmatrix} = \begin{bmatrix} S_{11} & S_{12} & S_{13} & 0 & 0 & 0 \\ S_{12} & S_{22} & S_{23} & 0 & 0 & 0 \\ S_{13} & S_{23} & S_{33} & 0 & 0 & 0 \\ 0 & 0 & 0 & S_{44} & 0 & 0 \\ 0 & 0 & 0 & 0 & S_{55} & 0 \\ 0 & 0 & 0 & 0 & 0 & S_{66} \end{bmatrix} \begin{Bmatrix} \sigma_1 \\ \sigma_2 \\ \sigma_3 \\ \tau_{23} \\ \tau_{31} \\ \tau_{12} \end{Bmatrix} \tag{3.1}$$

Here

$$S_{11} = \frac{1}{E_1}, \quad S_{12} = -\frac{\nu_{12}}{E_1} = -\frac{\nu_{21}}{E_2}, \quad S_{13} = -\frac{\nu_{13}}{E_1} = -\frac{\nu_{31}}{E_3}, \quad S_{23} = -\frac{\nu_{23}}{E_2} = -\frac{\nu_{32}}{E_3},$$

$$S_{22} = \frac{1}{E_2}, \quad S_{33} = \frac{1}{E_3}, \quad S_{44} = \frac{1}{G_{23}}, \quad S_{55} = \frac{1}{G_{31}}, \quad S_{66} = \frac{1}{G_{12}} \tag{3.2}$$

The strain-stress relations in Eq. 3.1 can be inverted to obtain the stress-strain relations:

$$\begin{Bmatrix} \sigma_1 \\ \sigma_2 \\ \sigma_3 \\ \tau_{23} \\ \tau_{31} \\ \tau_{12} \end{Bmatrix} = \begin{bmatrix} C_{11} & C_{12} & C_{13} & 0 & 0 & 0 \\ C_{12} & C_{22} & C_{23} & 0 & 0 & 0 \\ C_{13} & C_{23} & C_{33} & 0 & 0 & 0 \\ 0 & 0 & 0 & C_{44} & 0 & 0 \\ 0 & 0 & 0 & 0 & C_{55} & 0 \\ 0 & 0 & 0 & 0 & 0 & C_{66} \end{bmatrix} \begin{Bmatrix} \varepsilon_1 \\ \varepsilon_2 \\ \varepsilon_3 \\ \gamma_{23} \\ \gamma_{31} \\ \gamma_{12} \end{Bmatrix} \tag{3.3}$$

The stiffness matrix, C_{ij}, for an orthotropic materials in terms of the engineering constants, is obtained by inversion of the compliance matrix, S_{ij}. The stiffnesses in Eq. (3.3) are

$$C_{11} = \frac{1 - \nu_{23}\nu_{32}}{E_2 E_3 \Delta}, \qquad C_{22} = \frac{1 - \nu_{13}\nu_{31}}{E_1 E_3 \Delta}, \qquad C_{12} = \frac{\nu_{21} + \nu_{31}\nu_{23}}{E_2 E_3 \Delta} = \frac{\nu_{12} + \nu_{32}\nu_{13}}{E_1 E_3 \Delta},$$

$$C_{23} = \frac{\nu_{32} + \nu_{12}\nu_{31}}{E_1 E_3 \Delta} = \frac{\nu_{23} + \nu_{21}\nu_{13}}{E_1 E_2 \Delta}, \qquad C_{13} = \frac{\nu_{31} + \nu_{21}\nu_{32}}{E_2 E_3 \Delta} = \frac{\nu_{13} + \nu_{12}\nu_{23}}{E_1 E_2 \Delta},$$

$$C_{33} = \frac{1 - \nu_{12}\nu_{21}}{E_1 E_2 \Delta}, \qquad C_{44} = G_{23}, \qquad C_{55} = G_{31}, \qquad C_{66} = G_{12} \qquad (3.4)$$

where

$$\Delta = \frac{1 - \nu_{12}\nu_{21} - \nu_{23}\nu_{32} - \nu_{31}\nu_{13} - 2\nu_{21}\nu_{32}\nu_{13}}{E_1 E_2 E_3} \qquad (3.5)$$

3.2 Stress-Strain Relations for a Lamina of Arbitrary Orientation

In Section 3.1., the stresses and strains were defined in the principal material coordinates for an orthotropic material. However, the principal directions of orthotropy often do not coincide with coordinate directions that are geometrically natural to the solution of the problem. For this reason a method of transforming stress-strain relations from one coordinate system to another is needed.

The principal material axes and θ, is the angle from the x-axis to 1- axis, are shown in Figure 3. 1.

The stress transformations between x-y-z and 1-2-3 are,

$$\begin{Bmatrix} \sigma_{xx} \\ \sigma_{yy} \\ \sigma_{zz} \\ \sigma_{yz} \\ \sigma_{xz} \\ \sigma_{xy} \end{Bmatrix} = \begin{bmatrix} \cos^2\theta & \sin^2\theta & 0 & 0 & 0 & -\sin 2\theta \\ \sin^2\theta & \cos^2\theta & 0 & 0 & 0 & \sin 2\theta \\ 0 & 0 & 1 & 0 & 0 & 0 \\ 0 & 0 & 0 & \cos\theta & \sin\theta & 0 \\ 0 & 0 & 0 & -\sin\theta & \cos\theta & 0 \\ \sin\theta\cos\theta & -\sin\theta\cos\theta & 0 & 0 & 0 & \cos^2\theta - \sin^2\theta \end{bmatrix} \begin{Bmatrix} \sigma_1 \\ \sigma_2 \\ \sigma_3 \\ \sigma_4 \\ \sigma_5 \\ \sigma_6 \end{Bmatrix} \qquad (3.6)$$
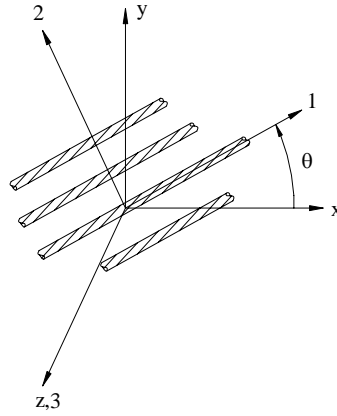
Figure 3. 1. Positive rotation of principal
materials axes from x-y-z axes

The strain-stress relations in x-y-z coordinates are,

$$
\begin{Bmatrix} \varepsilon_{xx} \\ \varepsilon_{yy} \\ \varepsilon_{zz} \\ \gamma_{yz} \\ \gamma_{xz} \\ \gamma_{xy} \end{Bmatrix} = \begin{bmatrix} \overline{S}_{11} & \overline{S}_{12} & \overline{S}_{13} & 0 & 0 & \overline{S}_{16} \\ \overline{S}_{21} & \overline{S}_{22} & \overline{S}_{13} & 0 & 0 & \overline{S}_{26} \\ \overline{S}_{31} & \overline{S}_{32} & \overline{S}_{33} & 0 & 0 & \overline{S}_{36} \\ 0 & 0 & 0 & \overline{S}_{44} & \overline{S}_{45} & 0 \\ 0 & 0 & 0 & \overline{S}_{45} & \overline{S}_{55} & 0 \\ \overline{S}_{16} & \overline{S}_{26} & \overline{S}_{36} & 0 & 0 & \overline{S}_{66} \end{bmatrix} \begin{Bmatrix} \sigma_{xx} \\ \sigma_{yy} \\ \sigma_{zz} \\ \sigma_{yz} \\ \sigma_{xz} \\ \sigma_{xy} \end{Bmatrix}
\tag{3.7}
$$

The transformed compliance coefficients $\overline{S}_{ij}$, referred to the (x, y, z) system,

$$
\begin{aligned}
\overline{S}_{11} &= S_{11} \cos^4 \theta - 2 S_{16} \cos^3 \theta \sin \theta + \left(2 S_{12} + S_{66}\right) \cos^2 \theta \sin^2 \theta - 2 S_{26} \cos \theta \sin^3 \theta \\
&\quad + S_{22} \sin^4 \theta
\end{aligned}
$$

$$
\begin{aligned}
\overline{S}_{12} &= S_{12} \cos^4 \theta + \left(S_{16} - S_{26}\right) \cos^3 \theta \sin \theta + \left(S_{11} + S_{22} - S_{66}\right) \cos^2 \theta \sin^2 \theta \\
&\quad + \left(S_{26} - S_{16}\right) \cos \theta \sin^3 \theta + S_{12} \sin^4 \theta
\end{aligned}
$$

$$
\overline{S}_{13} = S_{13} \cos^2 \theta - S_{36} \cos \theta \sin \theta + S_{23} \sin^2 \theta
$$

$$\bar{S}_{16} = S_{16}\cos^4\theta + (2S_{11} - 2S_{12} - S_{66})\cos^3\theta\sin\theta + 3(S_{26} - S_{16})\cos^2\theta\sin^2\theta$$
$$+ (S_{66} + 2S_{12} - 2S_{22})\cos\theta\sin^3\theta - S_{26}\sin^4\theta$$

$$\bar{S}_{22} = S_{22}\cos^4\theta + 2S_{26}\cos^3\theta\sin\theta + (2S_{12} + S_{66})\cos^2\theta\sin^2\theta + 2S_{16}\cos\theta\sin^3\theta$$
$$+ S_{11}\sin^4\theta$$

$$\bar{S}_{23} = S_{23}\cos^2\theta + S_{36}\cos\theta\sin\theta + S_{13}\sin^2\theta$$

$$\bar{S}_{26} = S_{26}\cos^4\theta + (2S_{12} - 2S_{22} + S_{66})\cos^3\theta\sin\theta + 3(S_{16} - S_{26})\cos^2\theta\sin^2\theta$$
$$+ (2S_{11} - 2S_{12} - S_{66})\cos\theta\sin^3\theta - S_{16}\sin^4\theta$$

$$\bar{S}_{33} = S_{33}$$

$$\bar{S}_{36} = 2(S_{13} - S_{23})\cos\theta\sin\theta + S_{36}(\cos^2\theta - \sin^2\theta)$$

$$\bar{S}_{44} = S_{44}\cos^2\theta + 2S_{45}\cos\theta\sin\theta + S_{55}\sin^2\theta$$

$$\bar{S}_{45} = S_{45}(\cos^2\theta - \sin^2\theta) + (S_{55} - S_{44})\cos\theta\sin\theta$$

$$\bar{S}_{55} = S_{55}\cos^2\theta + S_{44}\sin^2\theta - 2S_{45}\cos\theta\sin\theta$$

$$\bar{S}_{66} = S_{66}(\cos^2\theta - \sin^2\theta)^2 + 4(S_{16} - S_{26})(\cos^2\theta - \sin^2\theta)\cos\theta\sin\theta$$
$$+ 4(S_{11} + S_{22} - 2S_{12})\cos^2\theta\sin^2\theta \tag{3.8}$$

The stress-strain relations in x-y-z coordinates are,

$$
\begin{Bmatrix} \sigma_{xx} \\ \sigma_{yy} \\ \sigma_{zz} \\ \sigma_{yz} \\ \sigma_{xz} \\ \sigma_{xy} \end{Bmatrix} =
\begin{bmatrix}
\bar{C}_{11} & \bar{C}_{12} & \bar{C}_{13} & 0 & 0 & \bar{C}_{16} \\
\bar{C}_{21} & \bar{C}_{22} & \bar{C}_{23} & 0 & 0 & \bar{C}_{26} \\
\bar{C}_{31} & \bar{C}_{32} & \bar{C}_{33} & 0 & 0 & \bar{C}_{36} \\
0 & 0 & 0 & \bar{C}_{44} & \bar{C}_{45} & 0 \\
0 & 0 & 0 & \bar{C}_{45} & \bar{C}_{55} & 0 \\
\bar{C}_{16} & \bar{C}_{26} & \bar{C}_{36} & 0 & 0 & \bar{C}_{66}
\end{bmatrix}
\begin{Bmatrix} \varepsilon_{xx} \\ \varepsilon_{yy} \\ \varepsilon_{zz} \\ \gamma_{yz} \\ \gamma_{xz} \\ \gamma_{xy} \end{Bmatrix}
\tag{3.9}
$$

The transformed compliance coefficients $\overline{C}_{ij}$, referred to the (x, y, z) system,

$$\overline{C}_{11} = C_{11}\cos^4\theta - 4C_{16}\cos^3\theta\sin\theta + 2(C_{12}+C_{66})\cos^2\theta\sin^2\theta - 4C_{26}\cos\theta\sin^3\theta$$
$$+ C_{22}\sin^4\theta$$

$$\overline{C}_{12} = C_{12}\cos^4\theta + 2(C_{16}-C_{26})\cos^3\theta\sin\theta + (C_{11}+C_{12}-4C_{66})\cos^2\theta\sin^2\theta$$
$$+ 2(C_{26}-C_{16})\cos\theta\sin^3\theta + C_{12}\sin^4\theta$$

$$\overline{C}_{13} = C_{13}\cos^2\theta - 2C_{36}\cos\theta\sin\theta + C_{23}\sin^2\theta$$

$$\overline{C}_{16} = C_{16}\cos^4\theta + (C_{11}-C_{12}-2C_{66})\cos^3\theta\sin\theta + 3(C_{26}-C_{16})\cos^2\theta\sin^2\theta$$
$$+ (2C_{66}+C_{12}-C_{22})\cos\theta\sin^3\theta - C_{26}\sin^4\theta$$

$$\overline{C}_{22} = C_{22}\cos^4\theta + 4C_{26}\cos^3\theta\sin\theta + 2(C_{12}+2C_{66})\cos^2\theta\sin^2\theta$$
$$+ 4C_{16}\cos\theta\sin^3\theta + C_{11}\sin^4\theta$$

$$\overline{C}_{23} = C_{23}\cos^2\theta + 2C_{36}\cos\theta\sin\theta + C_{13}\sin^2\theta$$

$$\overline{C}_{26} = C_{26}\cos^4\theta + (C_{12}-C_{22}+2C_{66})\cos^3\theta\sin\theta + 3(C_{16}-C_{26})\cos^2\theta\sin^2\theta$$
$$+ (C_{11}-C_{12}-2C_{66})\cos\theta\sin^3\theta - C_{16}\sin^4\theta$$

$$\overline{C}_{33} = C_{33}$$

$$\overline{C}_{36} = (C_{13}-C_{23})\cos\theta\sin\theta + C_{36}(\cos^2\theta - \sin^2\theta)$$

$$\overline{C}_{44} = C_{44}\cos^2\theta + C_{55}\sin^2\theta + 2C_{45}\cos\theta\sin\theta$$

$$\overline{C}_{45} = C_{45}(\cos^2\theta - \sin^2\theta) + (C_{55}-C_{44})\cos\theta\sin\theta$$

$$\overline{C}_{55} = C_{55} \cos^2 \theta + C_{44} \sin^2 \theta - 2C_{45} \cos \theta \sin \theta$$

$$\overline{C}_{66} = 2(C_{16} - C_{26})\cos^3 \theta \sin \theta + (C_{11} + C_{22} - 2C_{12} - 2C_{66})\cos^2 \theta \sin^2 \theta$$
$$+ 2(C_{26} - C_{16})\cos \theta \sin^3 \theta + C_{66}(\cos^4 \theta + \sin^4 \theta)$$

(3.10)

Note that C_{14}, C_{15}, C_{16}, C_{24}, C_{25}, C_{26}, C_{34}, C_{35}, C_{36}, C_{45}, C_{46}, and C_{56} are zero for an orthotropic material.

3.3 Hashin Failure Criterion

Hashin failure criteria (1980) are polynominal failure criteria similar to the quadratic failure envelope except that in the Hashin formulation there are distinct polynomials corresponding to the different modes. Hashin-type failure criteria are ideal for use in finite element models, especially when adapted to progressive damage models. Hashin failure criterion reviewed above can be used to product fiber and matrix damaged modes. When a failure occurs in plane then the material properties in that location are degraded.

3.3.1 Hashin Criterion 3D (1980)

Tensile fiber mode

$$\left(\frac{\sigma_{11}}{X_T}\right)^2 + \frac{1}{S^2}\left(\sigma_{12}^2 + \sigma_{13}^2\right) = 1$$

(3.11)

or

$$\sigma_{11} = X_T$$

Compressive fiber mode

$$|\sigma_{11}| = X_C \tag{3.12}$$

Tensile matrix mode $(\sigma_{22} + \sigma_{33}) > 0$

$$\frac{1}{Y_T^2}(\sigma_{22} + \sigma_{33})^2 + \frac{1}{S_T^2}(\sigma_{23}^2 - \sigma_{22}\sigma_{33}) + \frac{1}{S^2}(\sigma_{12}^2 + \sigma_{13}^2) = 1 \tag{3.13}$$

Compressive matrix mode

$$\frac{1}{Y_C}\left[\left(\frac{Y_C}{2S_T}\right)^2 - 1\right](\sigma_{22} + \sigma_{33}) + \frac{1}{4S_T^2}(\sigma_{22} + \sigma_{33})^2 + \frac{1}{S_T^2}(\sigma_{23}^2 - \sigma_{22}\sigma_{33})$$

$$+ \frac{1}{S^2}(\sigma_{12}^2 + \sigma_{13}^2) = 1 \tag{3.14}$$

Here

X_T is the tensile strength of the fibers.

Y_T is the tensile strength in the transverse direction of the fibers.

X_C is the compressive strength of the fibers.

Y_C is the compression strength in the transverse direction of the fibers.

σ_{11} is the normal stress in the direction of the fibers of the lamina.

σ_{22}, σ_{33} are the normal stresses in the transverse directions to the fibers of the lamina.

σ_{23}, σ_{13}, σ_{12} are the shear stresses in the lamina.

S is the shear strength, in the 1-2 plane of the lamina.

S_T is the transverse shear strength in the 1-3 and 2-3 planes of the lamina.

CHAPTER FOUR

MODELLING AND SOLVING IN LUSAS

The opening screen of the lusas is for choosing the details of the model. We choose the unit as NmmtCs, startup template as composite and vertical axis as Z.
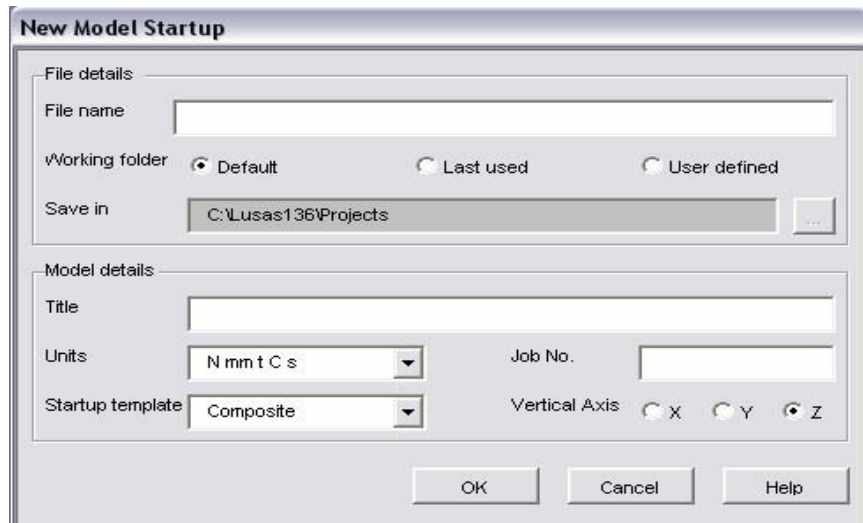
Figure. 4. 1. Starting menu.

Then we designate the center coordinates by clicking the new point button.
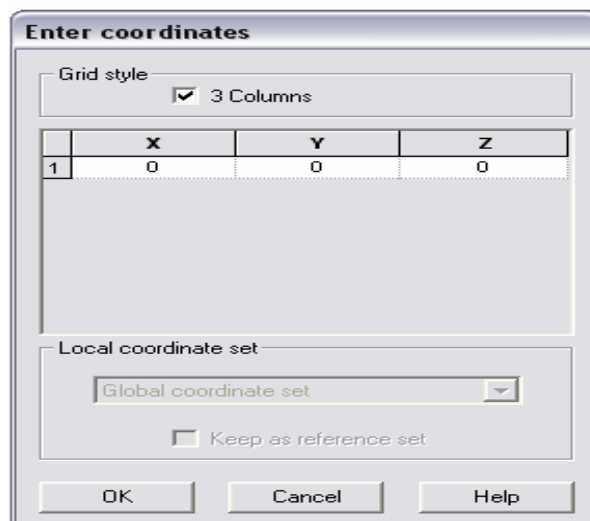
Figure. 4. 2. Center coordinates.

After creating the center point; we determine the coordinates of the quarter circle by clicking the new point button again. We can create new columns by pressing tab button.

Figure. 4. 3. Quater circle coordinates.

After choosing these three points, by clicking and holding the new line buton we choose the arc buton (Fig. 4. 4.) and draw the quarter circule (Fig. 4. 5.)

Figure. 4. 4. Drawing quarter circle
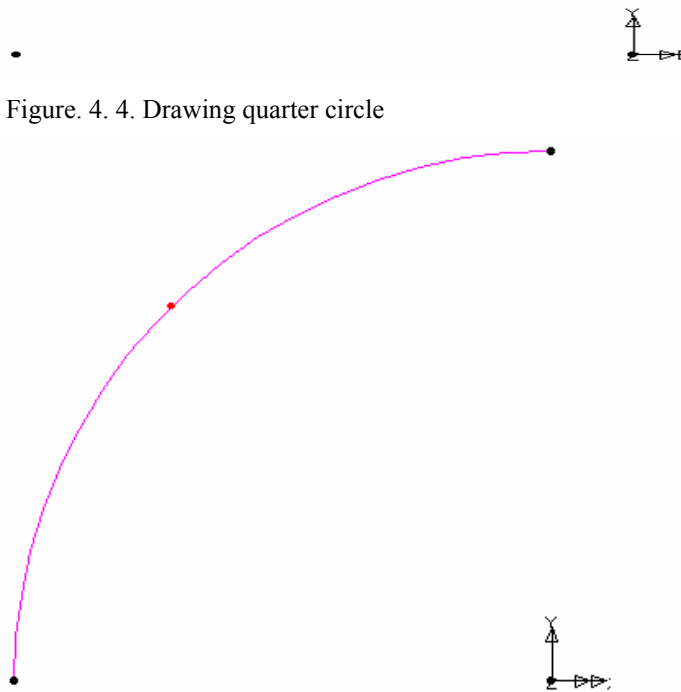
Figure.4.5. Quarter circle.

Using the same way we draw the half circle (Fig.4. 6.).
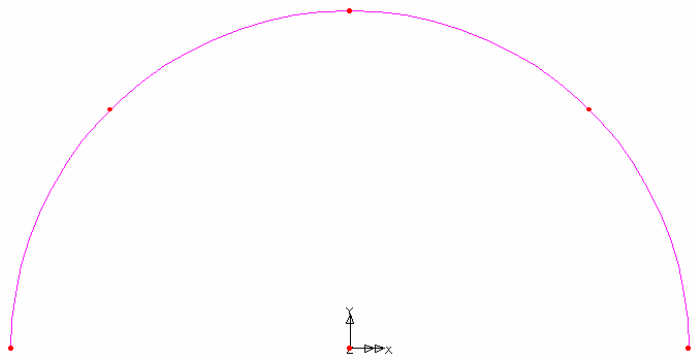
Figure. 4. 6. Half circle.

After this, using the split line evely button we divide the half circle into four parts. And then we determine the all points of the two dimensional model (Fig. 4. 7.).

Figure.4. 7. Entering all coordinates.
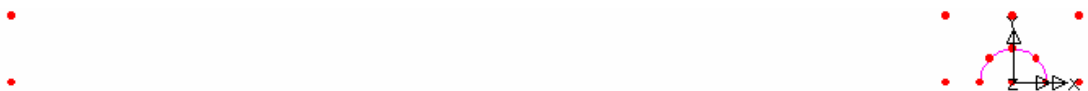
Figure. 4. 8. Points of two dimensional model.

We can now draw the two dimensional model by choosing two points and clicking the new line button.

Figure.4. 9. two dimensional model.

We should divide the part around the hole smaller pieces to make the analysis more satisfying (Fig. 4. 10.).

Figure. 4. 10. two dimensional model where the around area of the hole divided smaler parts.

When we complete the two dimensional model, we assign the line division to the whole model by pressing CTRL+A buttons (Fig .4. 11.).
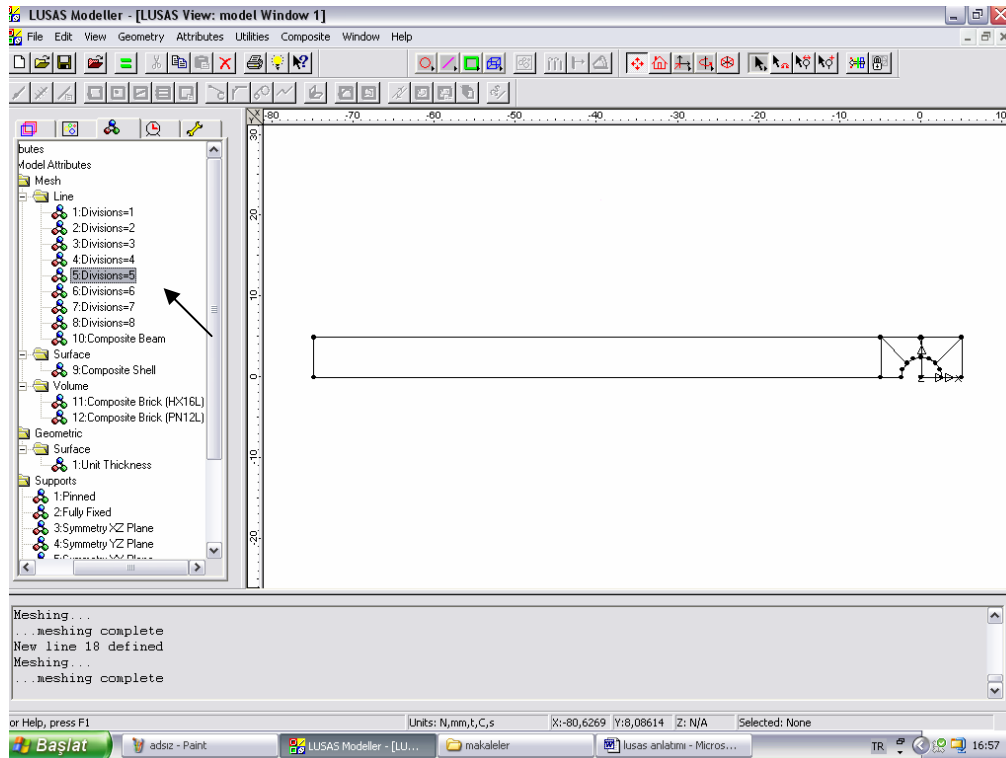
Figure. 4. 11. Line division.

Choosing the line form of the selection mode (Fig. 4.12.) we create surfaces (Fig.4.13.) by clicking the new surface button.
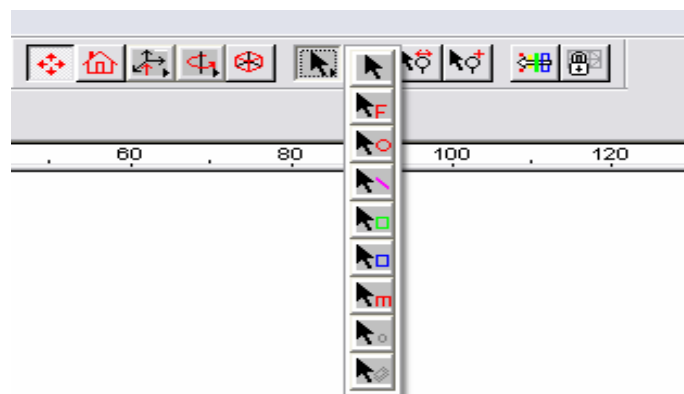
Figure. 4. 12. selection modes.

Figure. 4 13. Creating surfaces.

After creating all the new surfaces we chose the show surface axis from geometry (Fig. 4.14.).
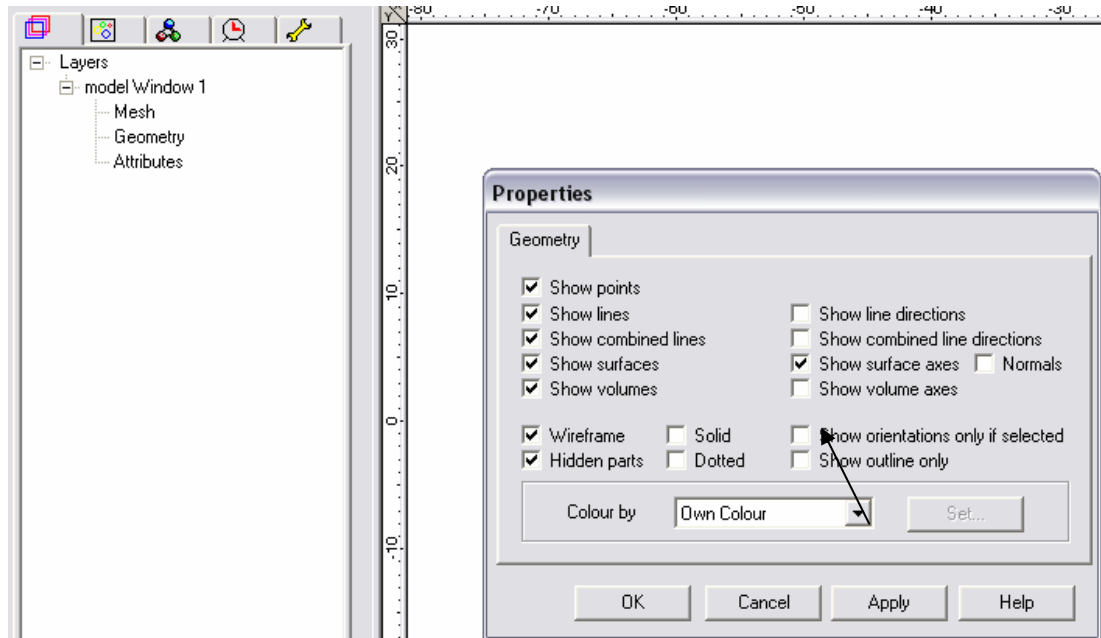
Figure. 4. 14. Showing surface axis.

Lusas determine the surface axes desultorily (Fig. 4.14.) because of this reason we should create a correct axes by using cycle definition button; after selecting this correct surface we choose the other surfaces, clicking the cycle relative button we correct all the surfaces (Fig. 4. 16.). Then we can desellect the show surface axes for a unadornate view.

Figure. 4. 15. Unsystematic surface axis.

Figure. 4 16. systematic surface axis

After proofreading the axes we create a three dimensional model by clicking the sweep feature button (Fig. 4.17.).
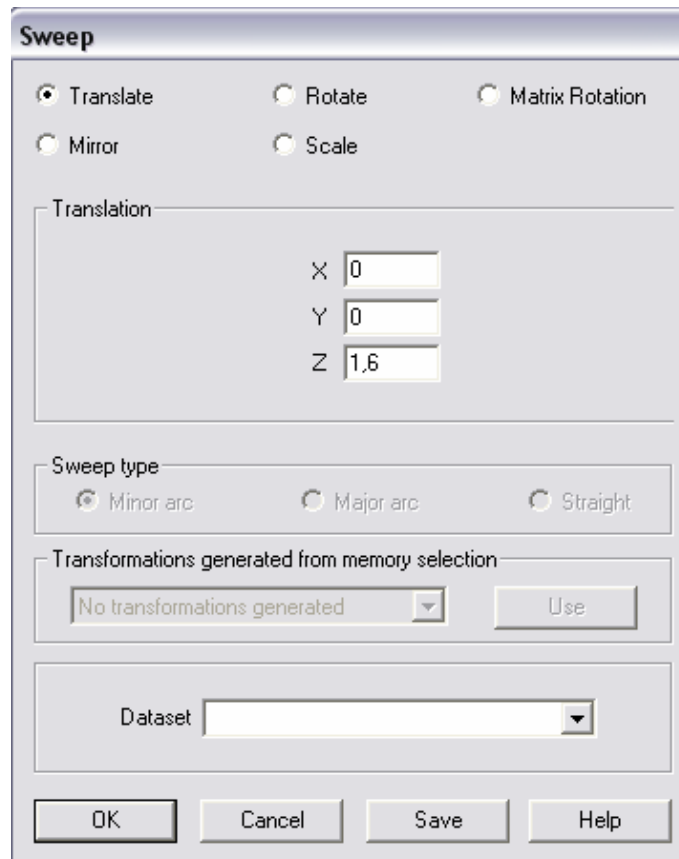
Figure. 4.17. Giving the thickness of the model.
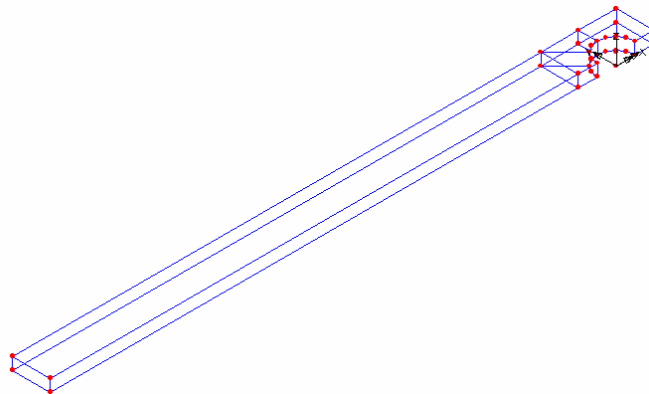
Figure. 4.18. Three dimensional model.

We click on the composite brick (HX16L) and chose allow transition pattern; then assign it to whole model (Fig . 4.19.). We should choose the default as 1 from FILE-MODEL PROPERTIES-MESHING.
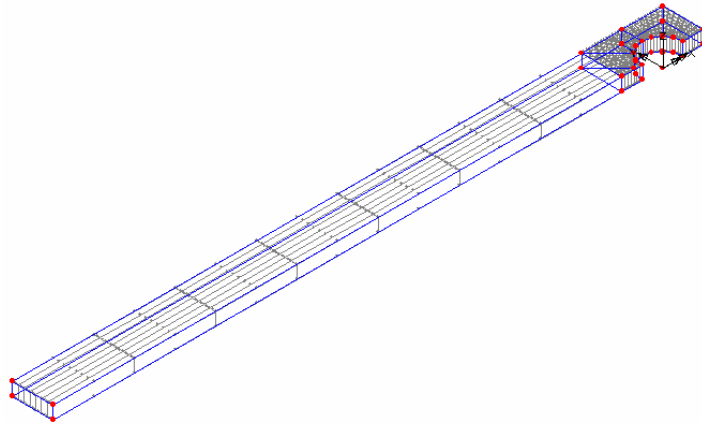
Figure. 4. 19. meshing of the model.

Later than this procedure we sign the failure criteria as Hashin from ATTRİBUTES-MATERİAL-COMPOSİTE LİBRARY (Fig.4. 20.).
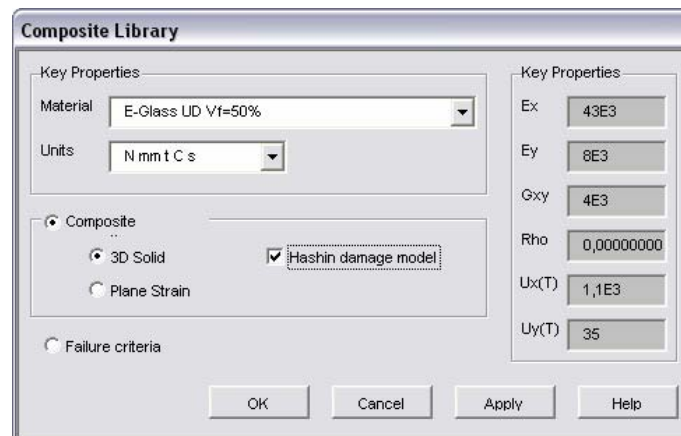
Figure. 4. 20. Choosing damage model.

Now we should define our materials characteristics by double clicking the E-Glass UD Vf=50% from the attributes window at the left part of the view (Fig.4.21.).
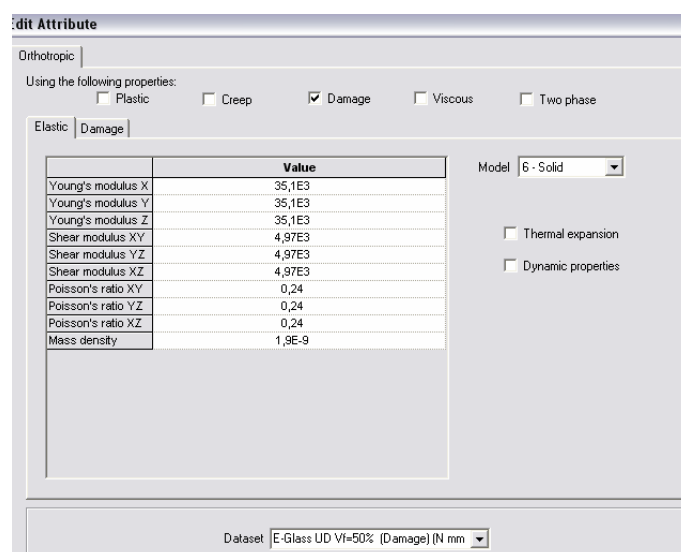
Figure. 4. 21. Composite material characteristics.

Our model is the half part of the whole model because of this reason we choose right surfaces of the model by using surface selection mode and appoint symmetry XZ plane to these surfaces (Fig. 4. 22.). Then we choose interior surface of the hole and choose cylindrical from ATTRIBUTES-LOCAL COORDİNATES and appoint this local coordinate to the interior wall of the hole; then click the fixed in X and appoint it to the same surfaces too (Fig. 4. 23.).
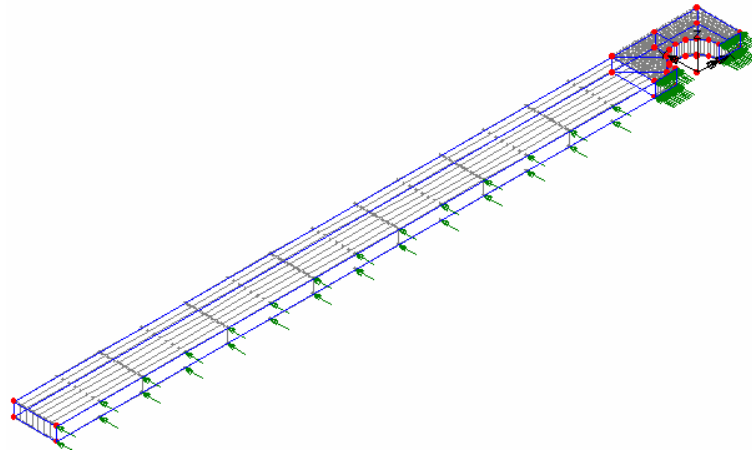
Figure. 4. 22. Symmetric surfaces.
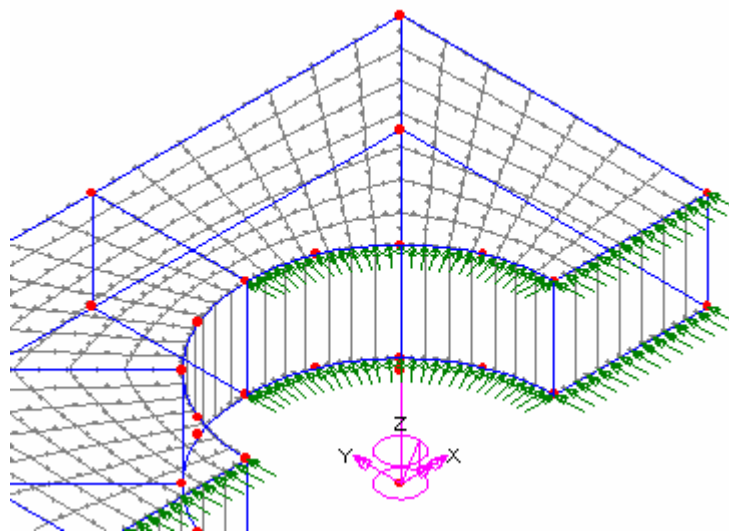
Figure. 4. 23. Creating the cylindrical coordinate.

To determine the load we lead the way, ATTIRIBUTES –LOADING-STRUCTURAL and define the load as shown in Fig.4. 24.
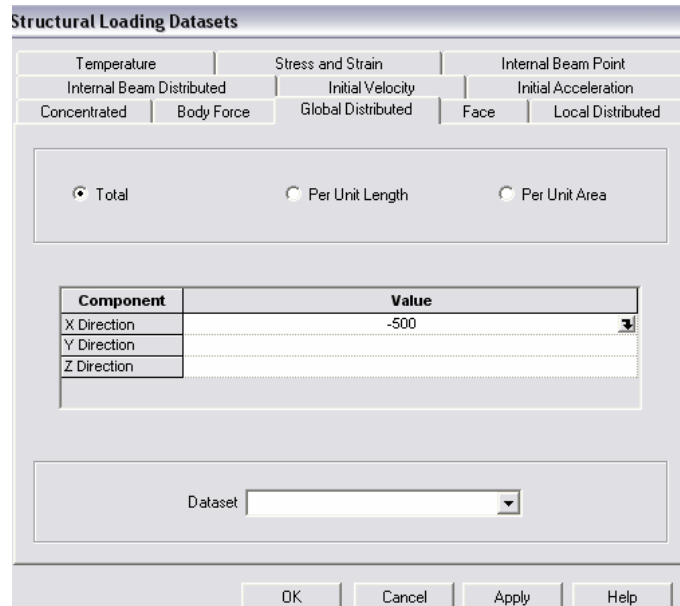
Figure. 4. 24. Structural loading dataset.
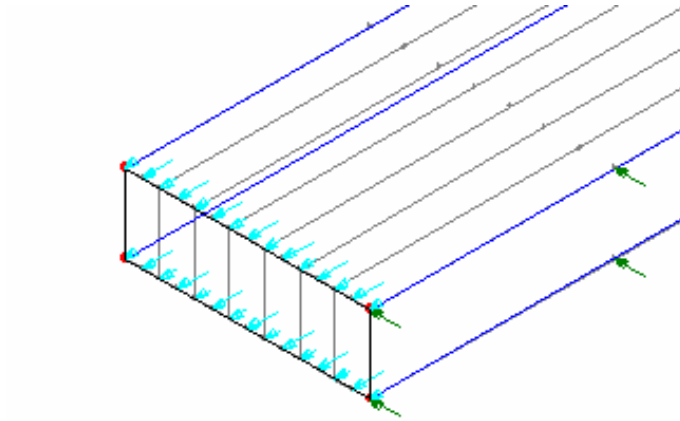
Figure. 4. 25. Structural load.

After this transaction we click load cases button at the left part of the screen then double click the load case 1 sign nonlinear & transient then click set and okay to determine our loading case. In this menu we choose incrementation as automatic; starting load factor as 1. Here starting load factor 1 represent 1000 N because our model is symmetric. We can choose other variables from this menu too as shown in Fig .4. 26.
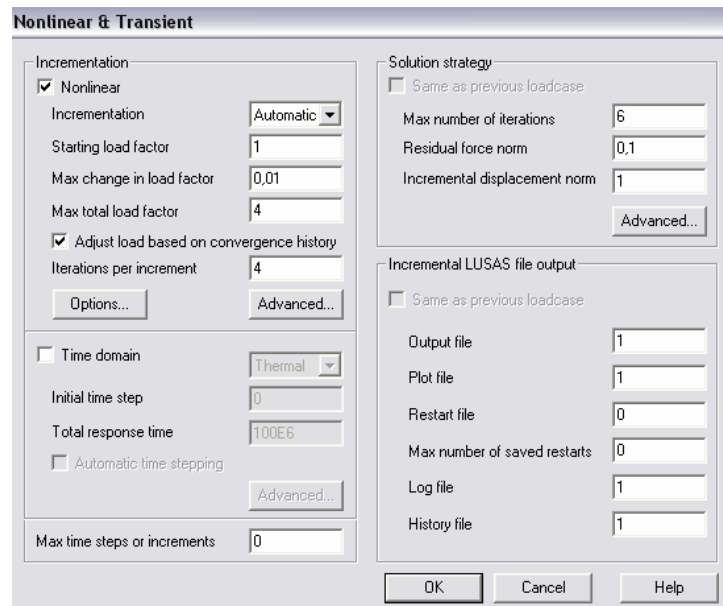
Fig .4. 26. Changing the variables of loadcase.

After designating the load case variables we sign the fine integration for mass (HX 16 and HX 20) from FILE- MODEL PROPERTIES-SOLUTION-ELEMENT OPTIONS. Then we define the failure strength from COMPOSITE-DEFINE FAILURE STRENGTH as shown in Fig. 4. 27. We should appoint all this transactions to the whole model.
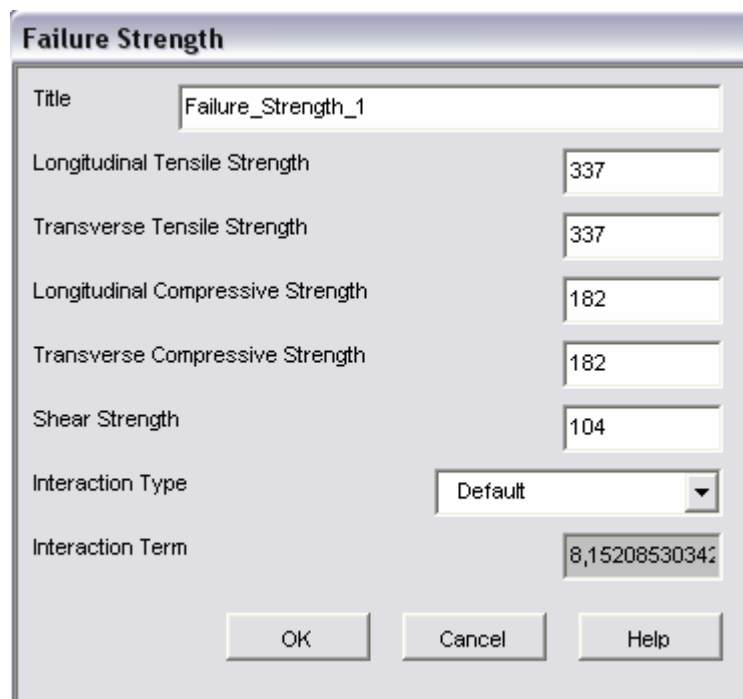
Figure. 4. 27. Failure strength.

Now our model is ready for solution. We can start the solution by clicking the solve now button. After computer finishes the solution we right click our mouse and sign the counter. From this menu we can choose the shape of the result as seen in Fig. 4. 28.
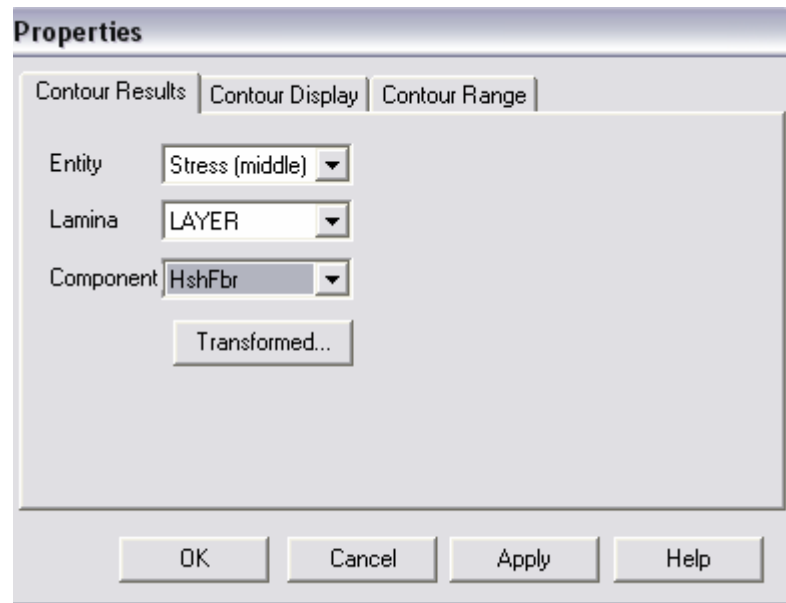
Figure. 4. 28. Solution properties.

CHAPTER FIVE
EXPERIMENTAL STUDY.

5. 1. Preparation of the composite plate

Composite material used in experiments was prepared in Izoreel Firm. At first one layer woven fiber-glass of 0.6 mm thickness and two layer aluminum plates of 0.5 mm thickness were cut at the same dimension. After this, mixed epoxy CY 225 and hardener HY 225 in the mass ratio 100:80; were spread two sides of woven fiber – glass; and at 120^0 temperature aluminum – glass epoxy-aluminum sandwich were pressed under 10 MPa pressure for 5 hours. The aluminum plates were manupulated by emery paper in order to obtain a good bonding between the aluminum plates and glass-epoxy plate.

The total thickness of the sandwich plate is 1.6 mm. The volume fraction of the woven glass-epoxy is measured as 60 %. Preparation of the sandwich plates is shown in Fig 5.1.
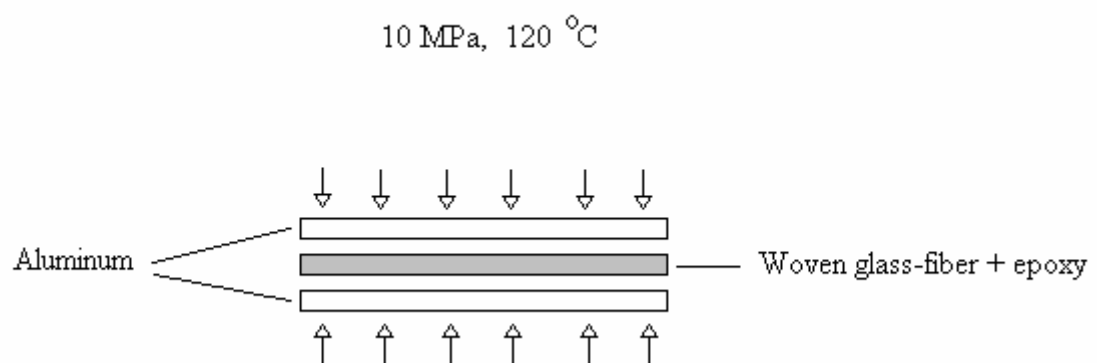
Figure. 5. 1. Preparation of sandwich plate.

5. 2. Material properties

Some mechanical tests were performed in order to calculate the mechanical properties and constants of the composite plate.

Because of the woven structure two fiber directions exists here Fig 5. 2; to obtain E_1, υ_{12} a rectangular specimen is taken which's one of the fiber direction coincides with the loading direction. And two strain gauges were stuck on perpendicular directions; one in loading direction and other in the transverse direction. The composite plate was loaded incrementally by an Instron – 1114 tensile machine and the strains ε_1, ε_2 were measured by an indicator. Then by using these strains E_1, υ_{12} were calculated.
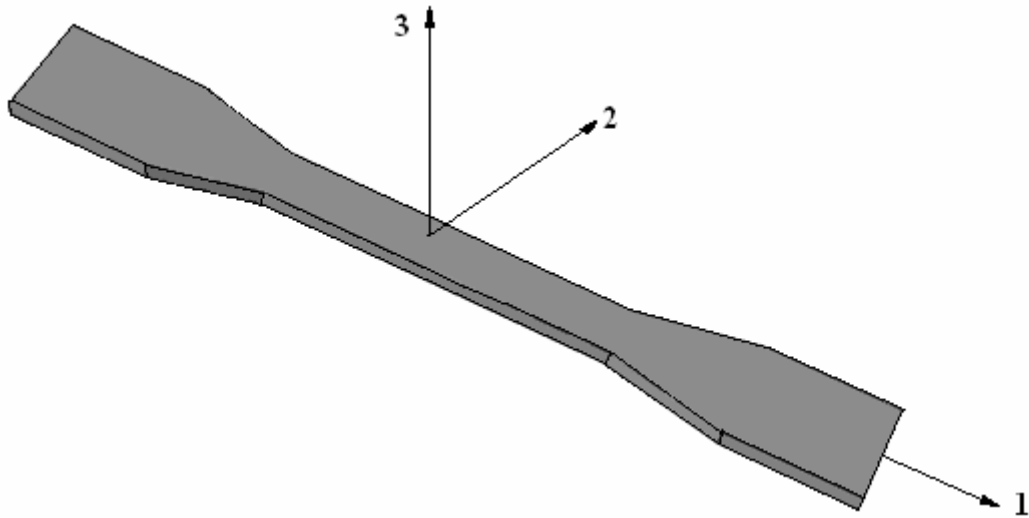
Figure. 5.2. Principal directions in a test specimen.

Load versus displacement diagram shown in Fig 5. 3 has two parts, first continues until yielding of the aluminum part and second part slope is lower than it. The specimen tears immediately at the ultimate force which is approximately two times higher than the yielding force so it can be said that glass-epoxy part increases the strength of the whole composite plate.
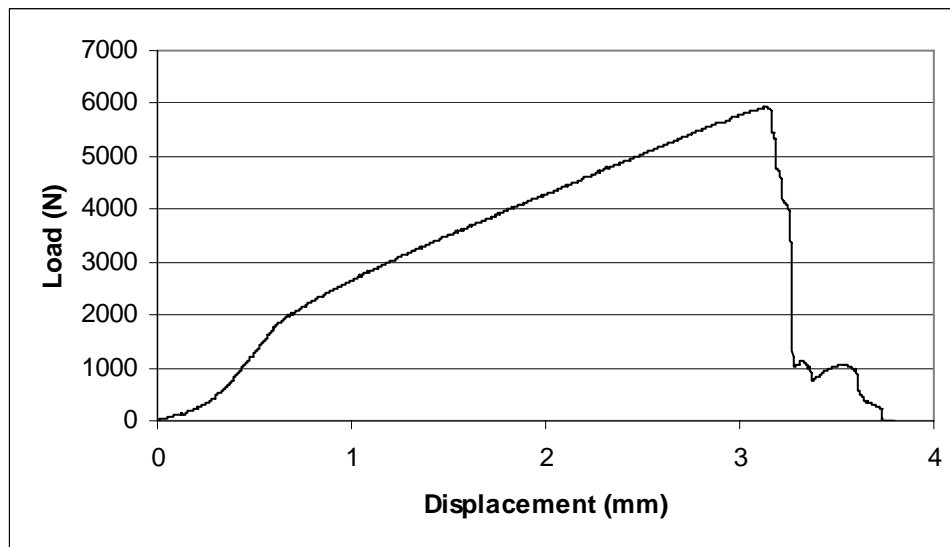
Figure. 5.3. Load versus displacement curve in a composite specimen.

Dividing the yield and the ultimate forces by cross sectional area gives the tensile strengths, X_y and X_t. After subjecting a specimen to compressive load which's one of the fiber direction coincides with the loading direction gives X_c by dividing the ultimate force by the cross-section area. A strain gauge was stuck on the loading direction of the lamina with an angle 45^0 one of the principal material directions for calculating the modulus of elasticity, in the loading direction. Then , the shear modulus G_{12} was calculated from formula 5.1 (Jones, R. M. 1999).

$$G_{12} = \frac{1}{\dfrac{4}{E_x} - \dfrac{1}{E_1} - \dfrac{1}{E_2} + \dfrac{2v_{12}}{E_1}}$$

(1)

To measure the shear strength S, Iosipescu testing method (Gibson, R. F. 1994) was used (Fig 5. 4.).
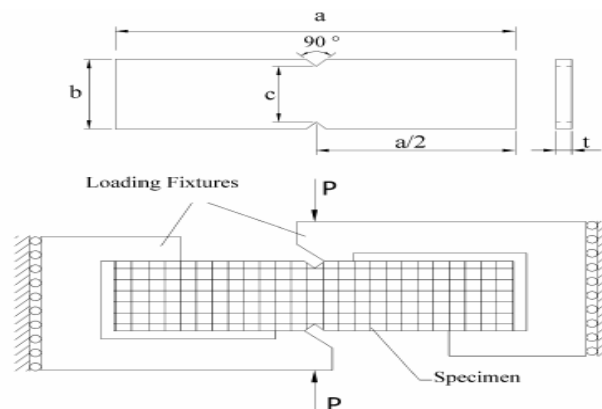
Figure. 5.4. Iosipescu test fixture.

Because of the woven structure E_2, Y_y, Y_t, Y_c are equal to E_1, X_y, X_t, X_c The mechanical properties are given in Table 5.1.

Table 5. 1. Mechanical properties of the aluminum glass-epoxy composite sandwich plate.

$E_1 = E_2$ (GPa)		35.10
G_{12} (GPa)		4.97
υ_{12}		0.24
$X_y = Y_y$ (MPa)		126
$X_t = Y_t$ (MPa)		337
$X_c = Y_c$ (MPa)		182
S (MPa)		104

5. 3. Problem statement

The composite rectangular plate is shown in Fig 5.5.
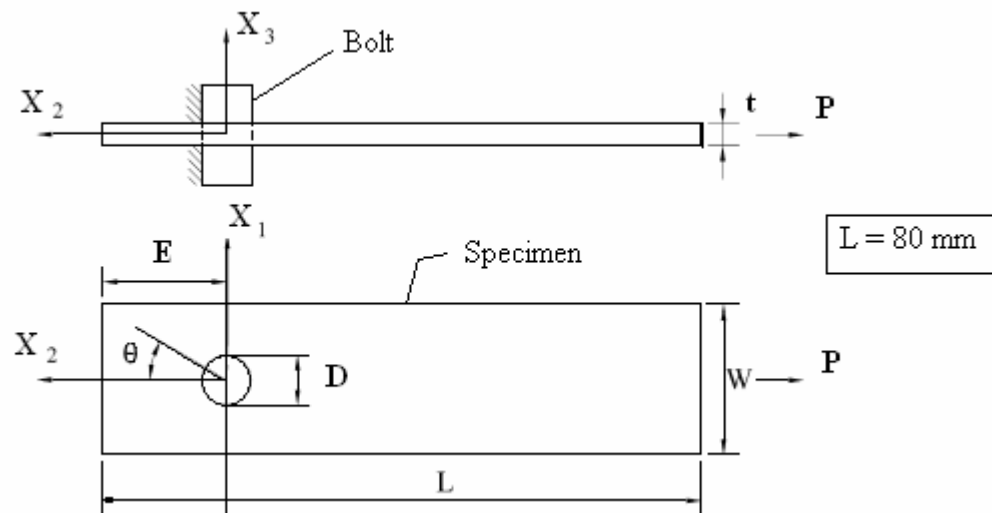
Figure. 5. 5. Geometry of the sandwich composite plate.

The tensile load P is parallel to the plate plane and symmetric with respect to the centerline for producing the uniform stress distribution in the plate. A pin or a bolt is located at the center of the hole and a uniform tensile load is applied to find the failure load and failure modes.

Net-tension, shear-out and bearing modes and their combinations are observed. The basic failure modes are shown in Fig. 5.(6-7-8).
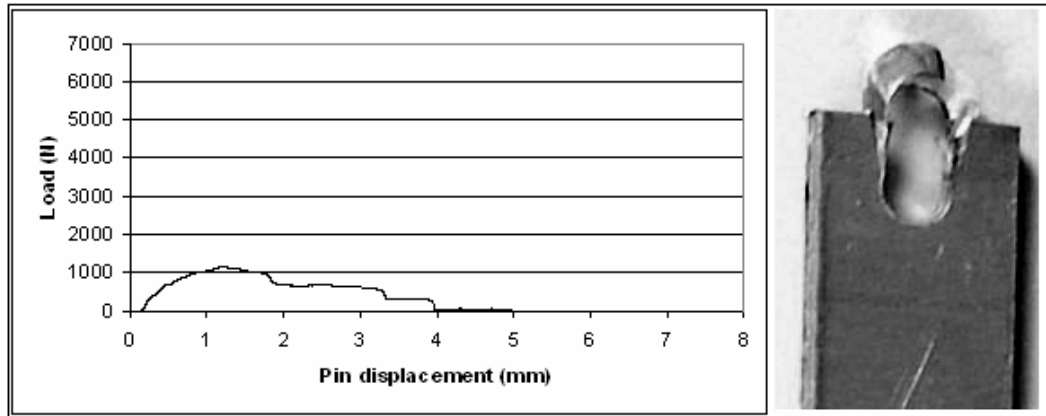
Figure. 5. 6. Shear-out failure mode.
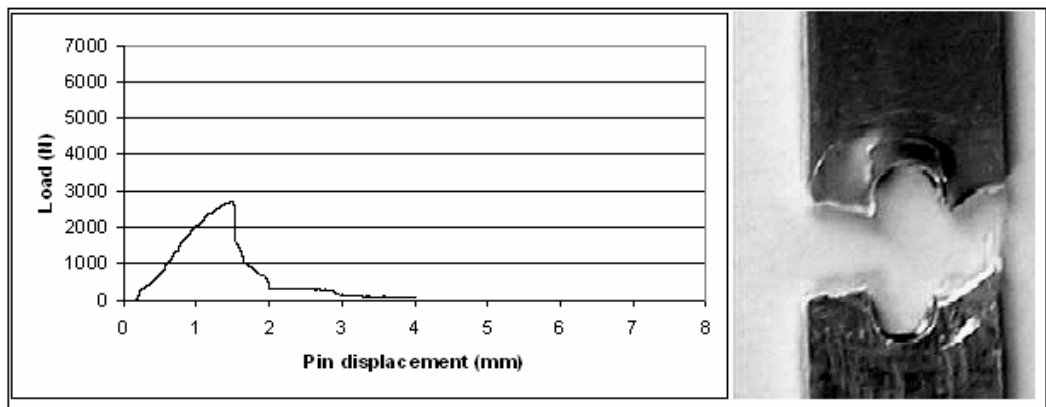
Figure. 5. 7. Net-tension failure mode.
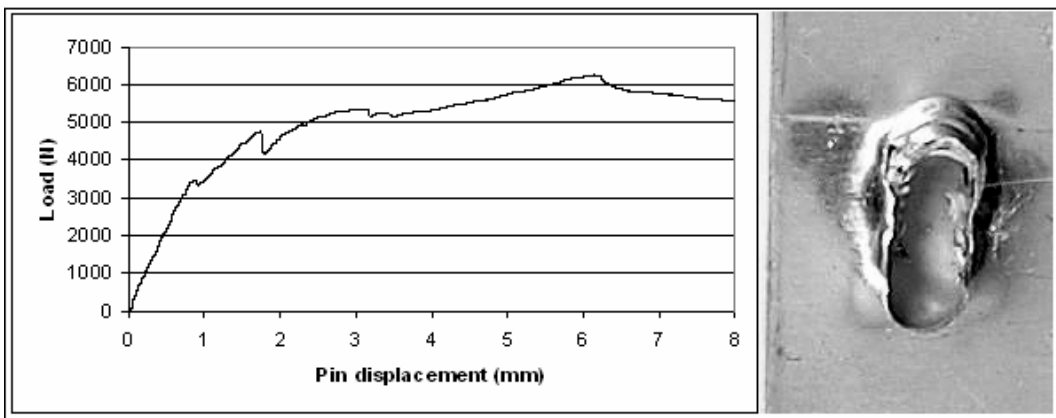
Figure. 5. 8. Bearing failure mode.

To find the bearing strengths formula 5. 2 is used as,

$$\sigma_b = \frac{P}{D.t}$$

(5.2)

Here P is the load, D and t are the diameter and the thickness of the composite plates, respectively. Also metric 5 bolts suitable for the experimental setup was produced.

5. 4 . Specimen preparation

The specimens were trimmed and 5 mm holes were drilled. The effect of preload and pin location were studied by varying the preload moment M = 0-3-6 Nm; end distance to diameter ratio (E/D) from 1 to 5 and width to diameter ratio (W/D) from 2 to 5 with a constant thickness t of 1.6 mm and a constant length 80 mm.

Two experimental setup's were used for this study. The first one was for experiments subjected by a bolt impacted by a preload and a washer Fig 5.9; the other was for pinned –joint experiments where M = 0 Nm prepared for the study of ICTEN and SAYMAN Fig. 5.10 . The Instron-1114 tensile machine was worked at a crosshead speed of 1 mm/min and 15 mm washers was used for preload.
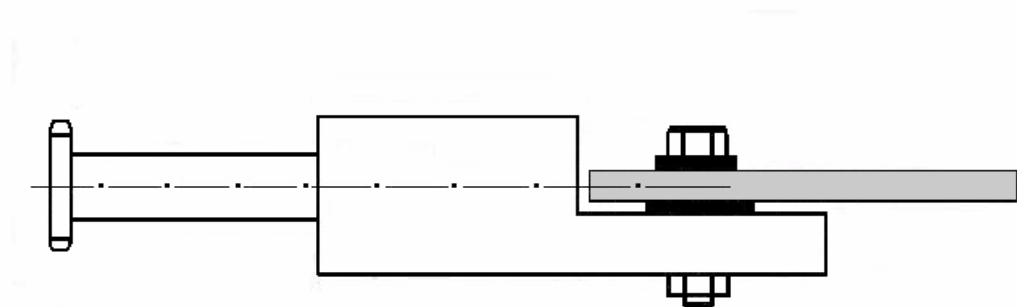
Figure. 5. 9. Experimental setup for a bolted sandwich composites with a preload.
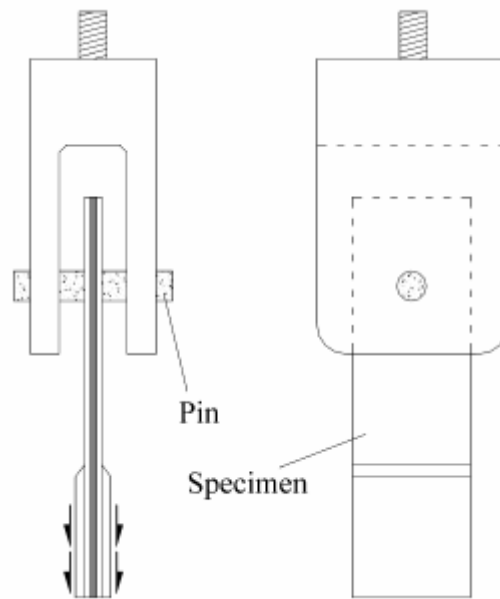
Figure. 5.10. Experimental setup for the pinned-joint
fixture

CHAPTER SIX
NUMERICAL STUDY

6.1 Introduction

A static progressive failure analysis was performed on sixty different bolted composite plates by using LUSAS 13.6 finite element analysis program. In addition, parametric studies have been performed using various geometry. The effects of material non-linearity on the prediction of the failure initiation and failure loads were studied.

6.2 Three-dimensional finite element method

In the three-dimensional finite element formulation, the displacements, traction components, and distributed body force values are the functions of the position indicated by (*x, y, z*). The displacement vector **u** is given as

$$\mathbf{u} = [u, v, w]^T \tag{6.1}$$

where *u,* v and w are the *x, y* and *z* components of **u**, respectively. The stress and strains are given by

$$\sigma = [\sigma_{xx}, \sigma_{yy}, \sigma_{zz}, \sigma_{yz}, \sigma_{xz}, \sigma_{xy}]^T$$
$$\varepsilon = [\varepsilon_{xx}, \varepsilon_{yy}, \varepsilon_{zz}, \gamma_{yz}, \gamma_{xz}, \gamma_{xy}]^T \tag{6.2}$$

From Figure 6.1, representing the three- dimensional problem in a general setting, the body force and traction vector are given by

$$\mathbf{f} = [f_x, f_y, f_z]^T \quad , \quad \mathbf{T} = [T_x, T_y, T_z]^T \tag{6.3}$$

The body force **f** has dimensions of force per unit volume, while the traction force

T has dimensions of force per unit area.
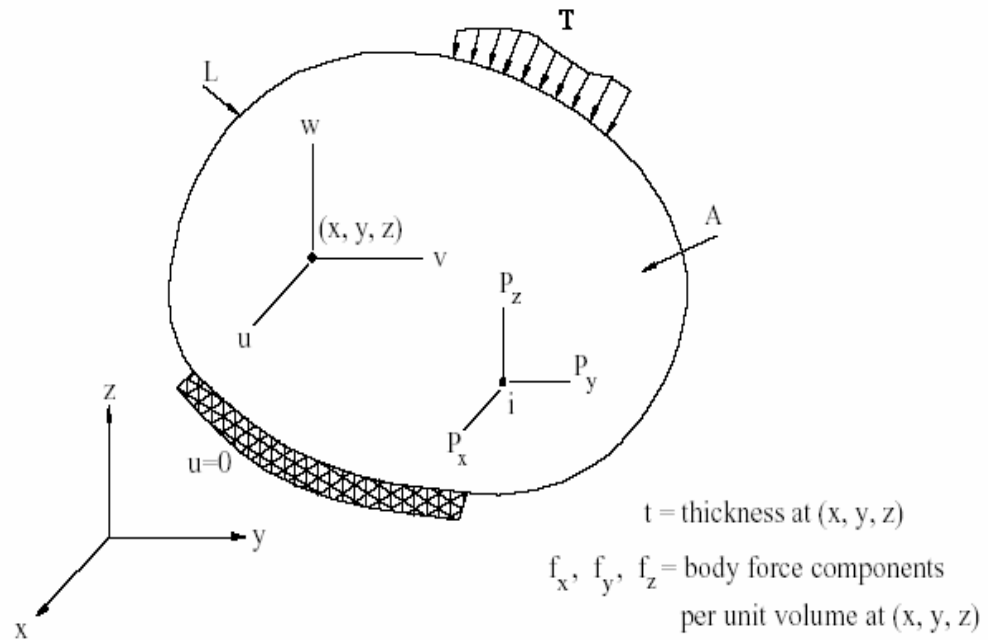
Figure. 6. 1. Three-dimensional problem

6.3 Modeling of the problem.

Solution of specimens without a preload was explained in modeling and solving in lusas part. In this chapter; the failure analysis of specimens with a preload moment (M = 3 Nm , M = 6 Nm) is given.

For the specimens with a preload moment we should create a rectangular surface which's area is equal to the washer (Fig. 6.2); here this area is shown with the red lines.
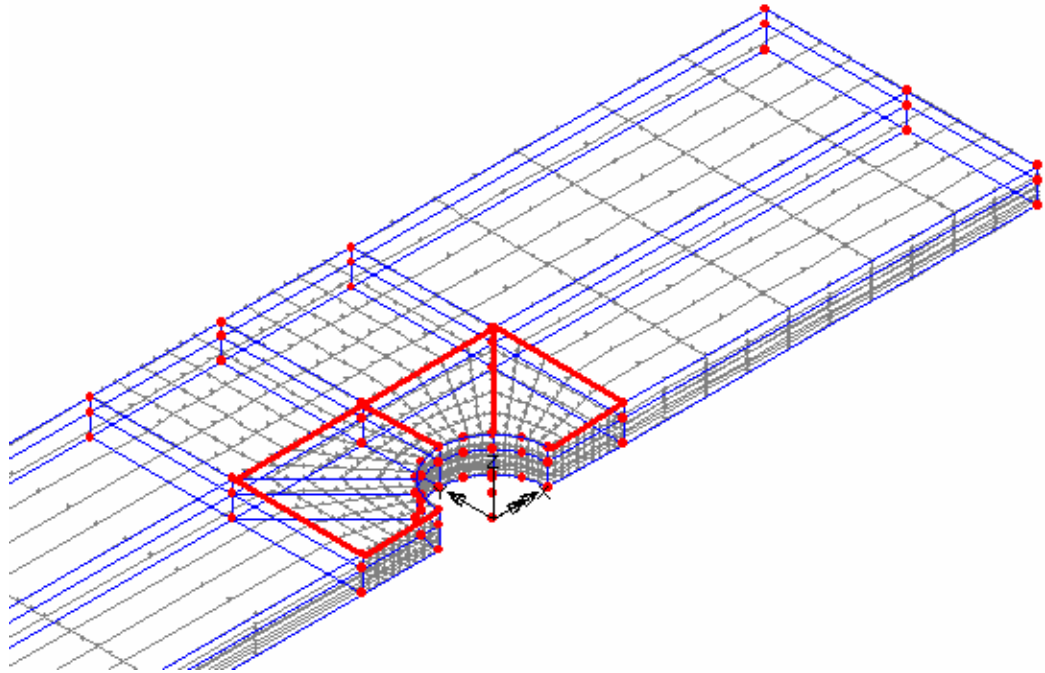
Figure. 6.2. Creating an area equal to the washer's area.

Then we apply the friction force and the normal force at this area as shown in Fig. 6. 3.
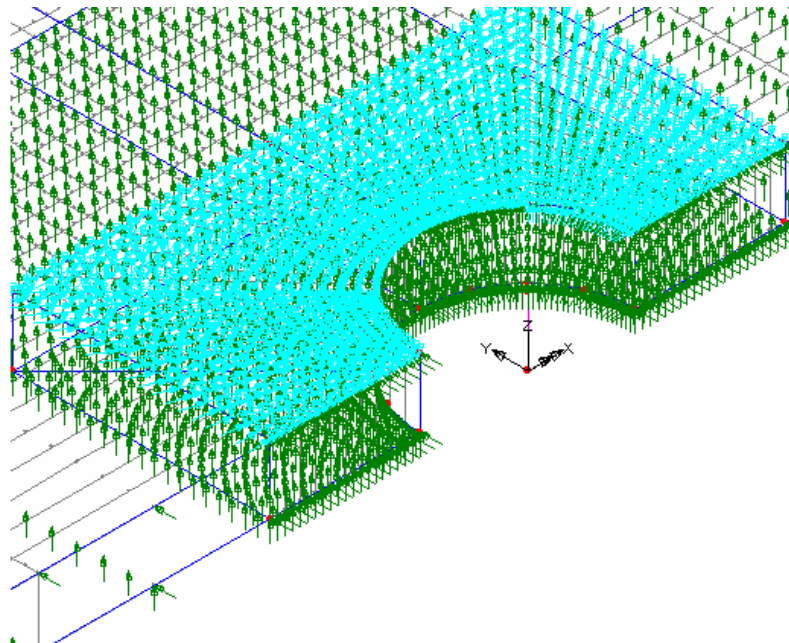
Figure. 6. 3. Friction and normal force on the created area.

Because of the normal force applied, we must fix our model in the Z direction by selecting the whole surfaces in the Z direction and appoint the fixed in Z to these surfaces(Fig. 6. 4).
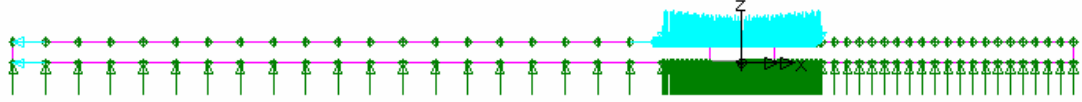
Figure. 6. 4. Fixing the model in Z direction.

Here while modeling the plate we must choose the points symmetric to each other (Fig. 6.5); because of this reason two surfaces appeared in tensile direction so we should divide the applied force to these surfaces proportional with their area individual (Fig. 6. 6). In this figure the surfaces shown with red and yellow lines.
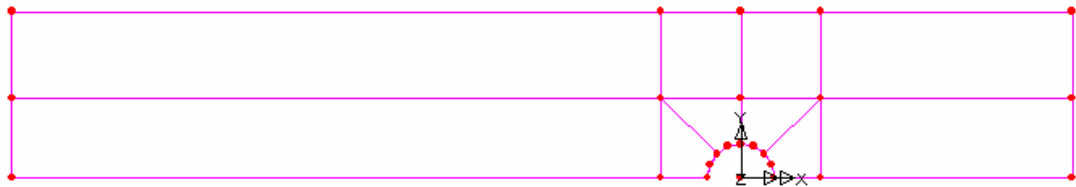
Figure. 6.5. Symmetric points in a specimen with a preload moment.
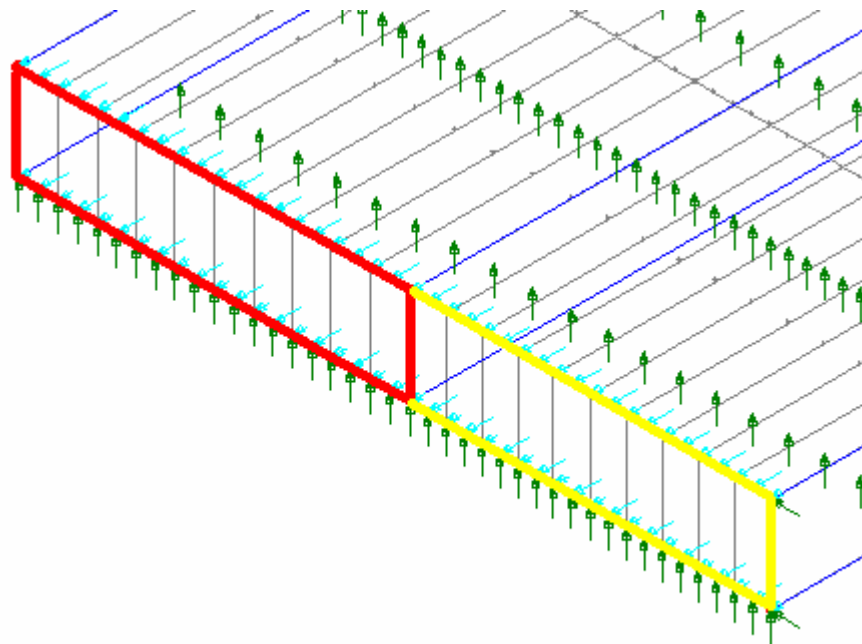
Figure. 6. 6. Separated areas in the tensile direction

CHAPTER SEVEN
RESULTS AND DISCUSSION

Each composite joint was loaded until the tear occurred. The general behavior of the composite joint was obtained from the load-displacement curves.

7. 1. Width to diameter ratio (W/D)

The shear-out failure mode is observed at E/D = 1, for all the W/D ratios and under preload moments as shown in Figure 7.1. a. When both E/D and W/D reach 2, the plate is still weak and the failure mode is the net-tension, as shown in Figure 7. 1. d. As seen in these Figures, the preload moments affect the applied force (P). When the preload moment is increased, the applied force (P) attains the high values. Increasing of W/D ratio increases the bearing strengths. The combinations of failure modes are seen for W/D = 3 and 4 as shown in Figures 7. 1. ı-n-o. As seen in these Figures the large values of preload moments produce the high failure strengths.

The full bearing-failure mode occurs at W/D = 5, as illustrated in Figures 7. 1. s-u. As seen in these Figures, the failure mode reaches the high values for the large values of the preload moment, because the preload moment and as a result of the surface and frictional forces increase the failure strengths.

7.2 End distance to diameter ratio (E/D)

When the ratio of E/D is taken as a constant value and the ratio of W/D is changed, the failure mode of the plates varies. The shear-out failure mode occurs for E/D = 1 for all W/D ratios an all the values of preload moment as shown in Figure 6. 2. a. E/D ratio affects the failure modes, as shown in Figures 7. 2. b-c-d-e. As seen in these Figures that, increasing of E/D ratio produces the bearing failure modes and increases the bearing strength. All the experiments for E/D = 1 represent shear-out

failure mode however for other values net-tension, bearing and combinations seen depend on the change of width and preload moment as shown in Figure 7. 3. As seen in these Figures if W/D and E/D both are increased bearing strength values reach high values. The values of preload moments affect the bearing strengths. They reach the highest values for M = 6 Nm moment. At the same time the values for 3 Nm are higher than those for without preload moment.

7.3 Preload moment

When the effects of preload moment over specimens are examined on the failure mode of the composite plate, it is seen that the preload increases the failure strength of the plate. Since the preload moment produces the friction force which is caused by the normal force on the washer and specimen; it has a great effect on the failure mode and strength of the plate, as shown in Figure 7. 1. a. It is seen in this Figure that, although the shear-out failure is observed, the failure load increases at the high premoments because of the clamping pressure of the washer.

The friction and the compression forces due to preload moment connect the plates, washer and nuts and then the washer, nut and bolt carry a great part of the applied force. As a result of this, the effect of the applied force on the composite plate decreases and then the failure strength increases as shown in Figures 7.2 and 7. 3.

Preload moments affect the shape of failure modes as seen at Table 7. 1. As seen in this table the preload moment changes the modes of the failure in a small range. As seen in Figure 7. 1. the combinations of E/D, W/D, and preload moments affect the failure strength. If they are all together increased, the failure strength increases. For instance E/D = 1, W/D = 5 and M = 3 Nm the failure strength is 300 MPa, however for E/D = 5, W/D = 5 and M = 6 Nm the failure strength is 784 MPa. If the premoment is applied to the plates, the failure stress increases about 2 times for M = 0 Nm and M = 6 Nm respectively.

a)

W/D = 2 E/D = 1

b)

W/D = 2 , E/D = 2

c)

W/D = 2 , E/D = 3

d)

W/D = 2 E/D = 4

e)

W/D = 2 , E/D = 5

f)

W/D = 3 , E/D = 1

g)

W/D = 3 , E/D = 2

h)

W/D = 3 , E/D = 3

1)

W/D = 3 E/D = 4

j)

W/D = 3 , W/D = 5

k)

W/D = 4 , E/D = 1

l)

W/D = 4 , E/D = 2

m)

W/D = 4 , E/D = 3

Load (N) vs Pin displacement (mm)

n)

W/D = 4 E/D =4

Load (N) vs Pin displacement (mm)

o)

W/D = 4 E/D = 5

Load (N) vs Pin displacement (mm)
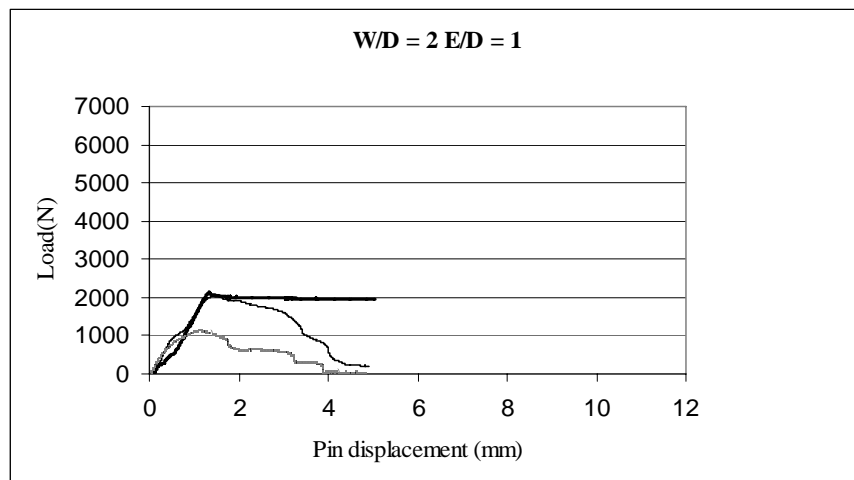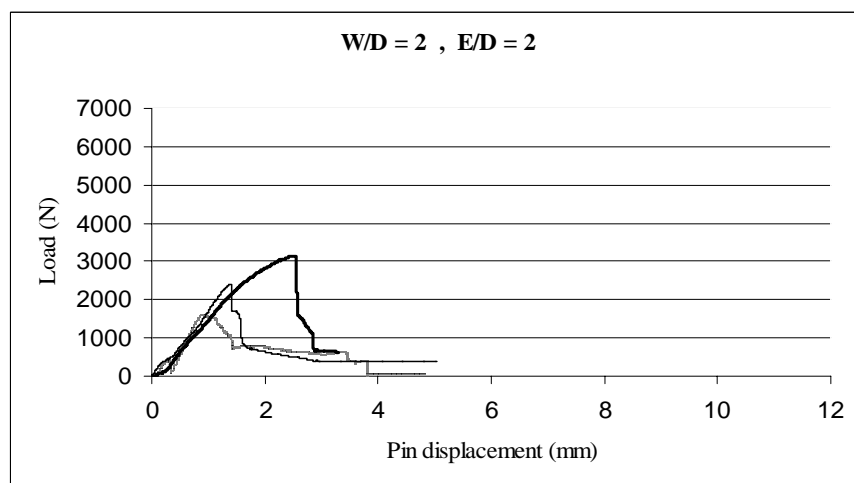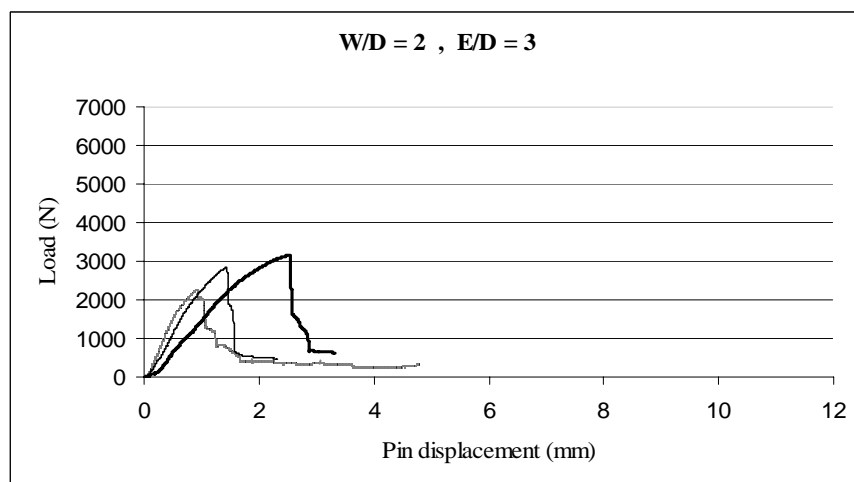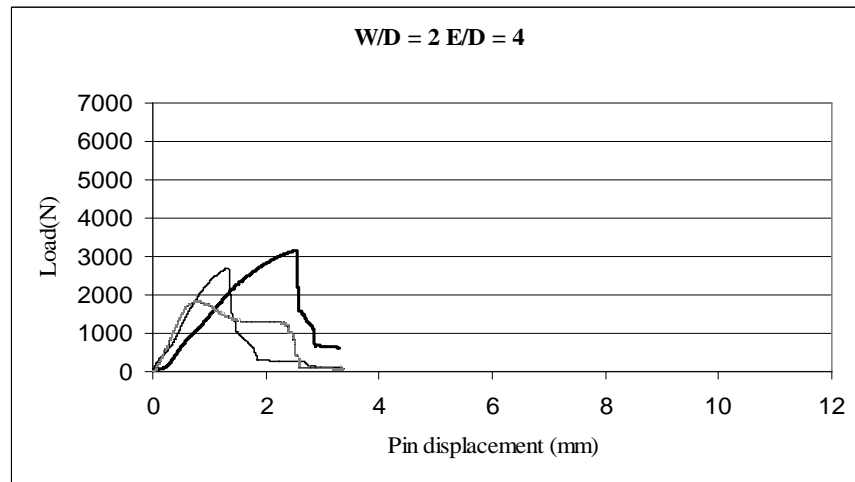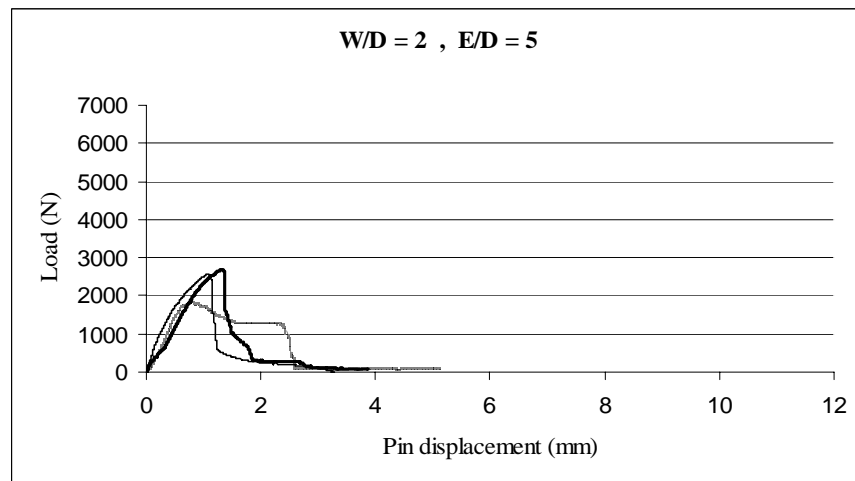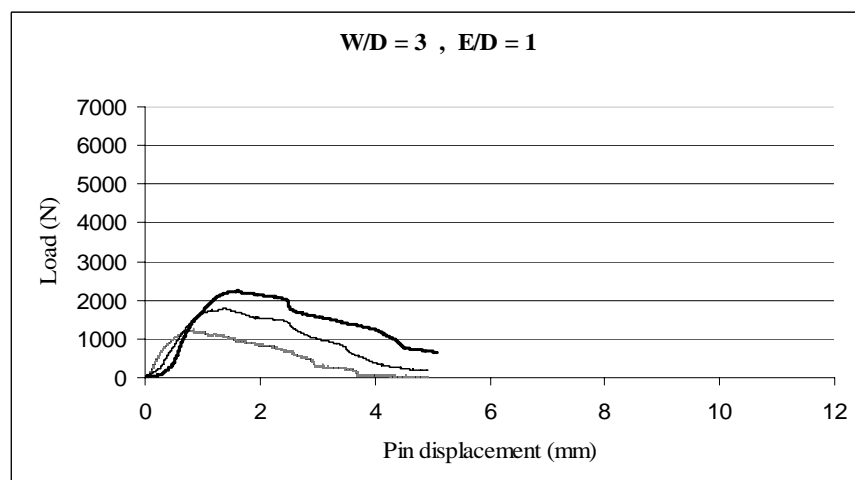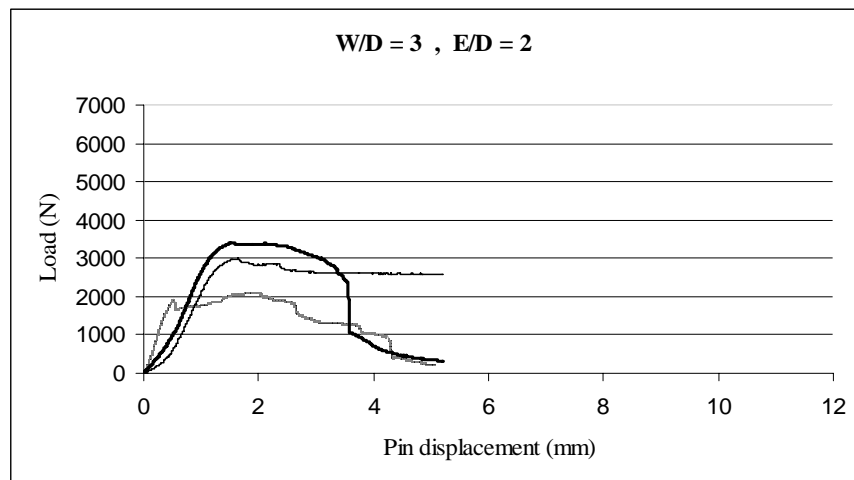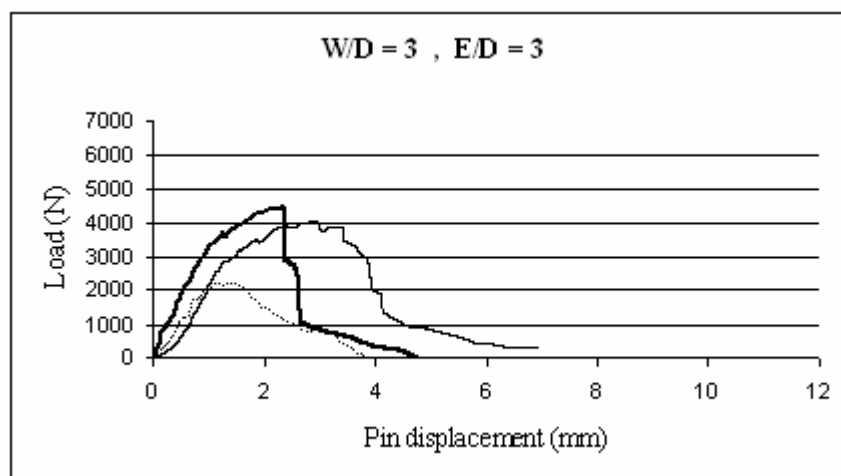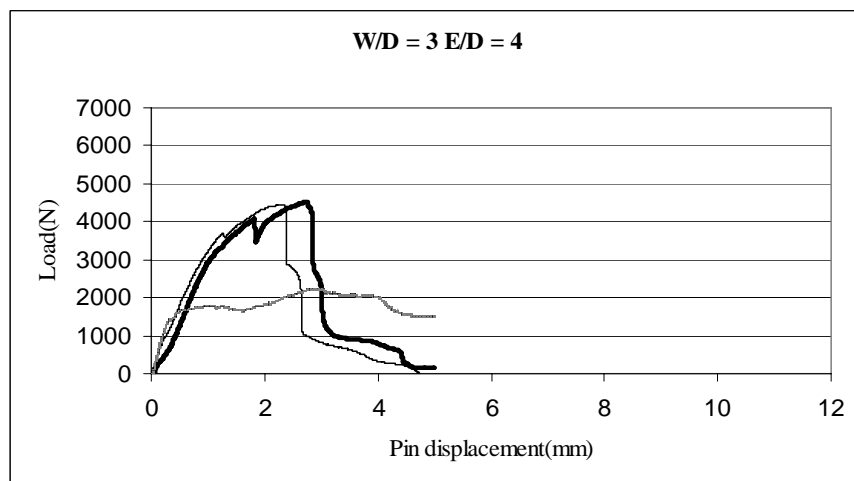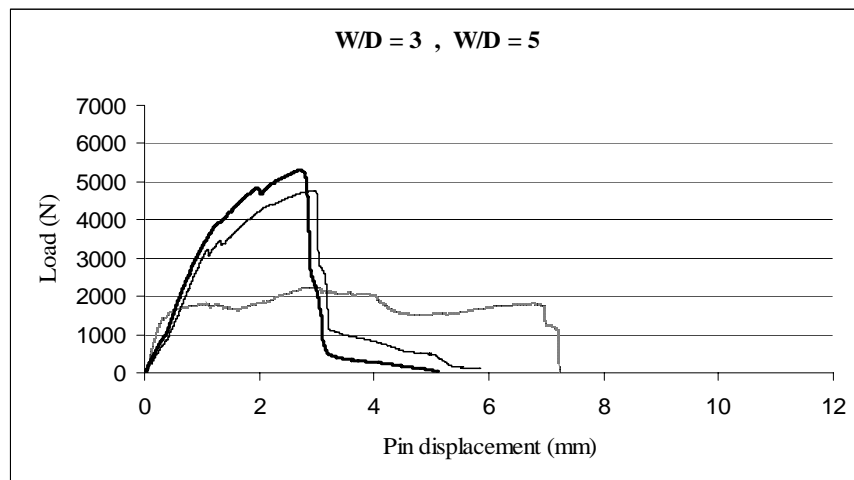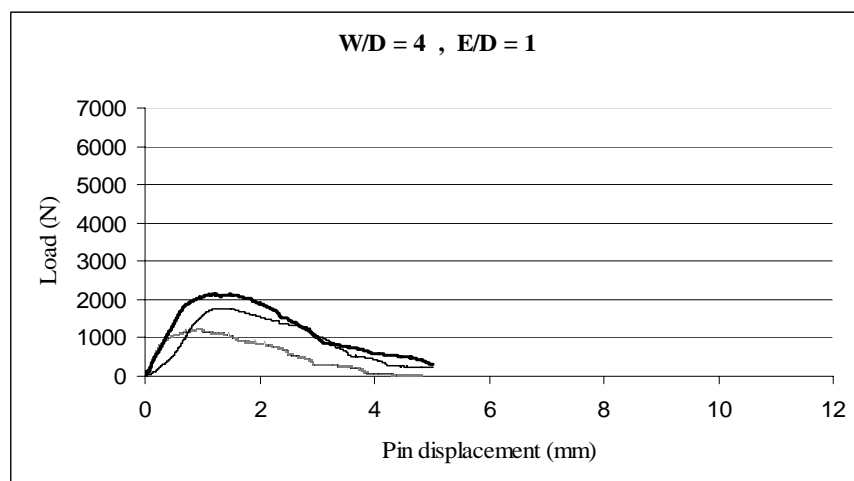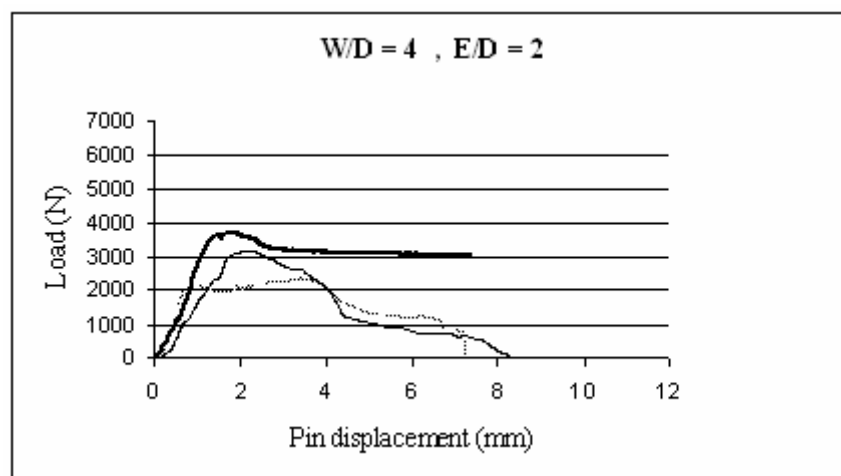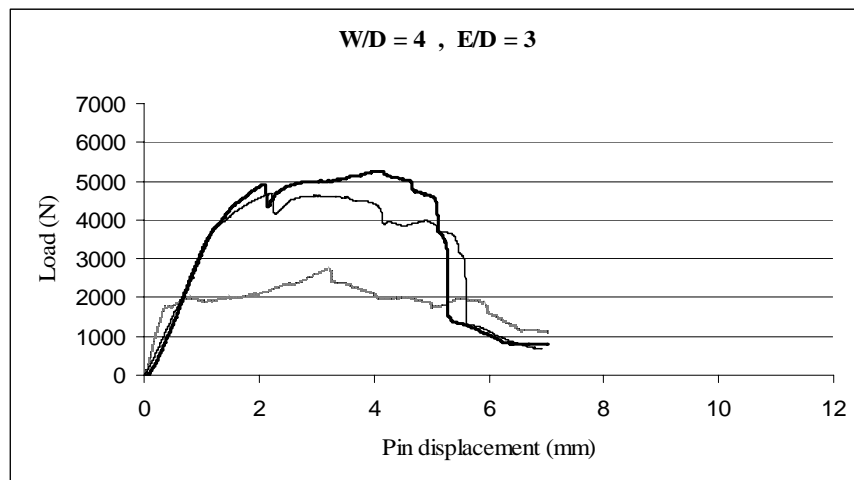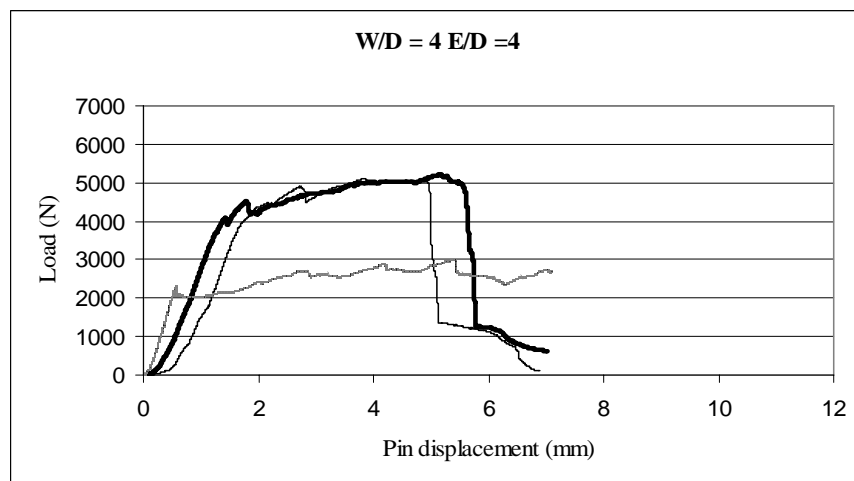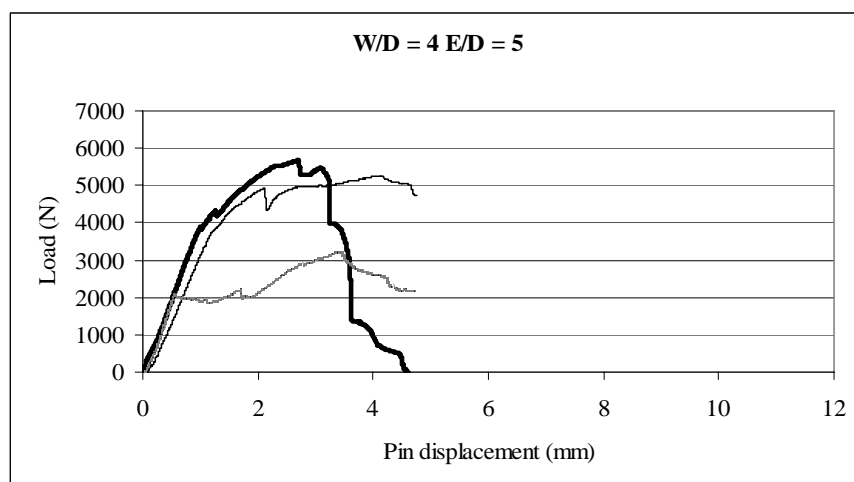
p)
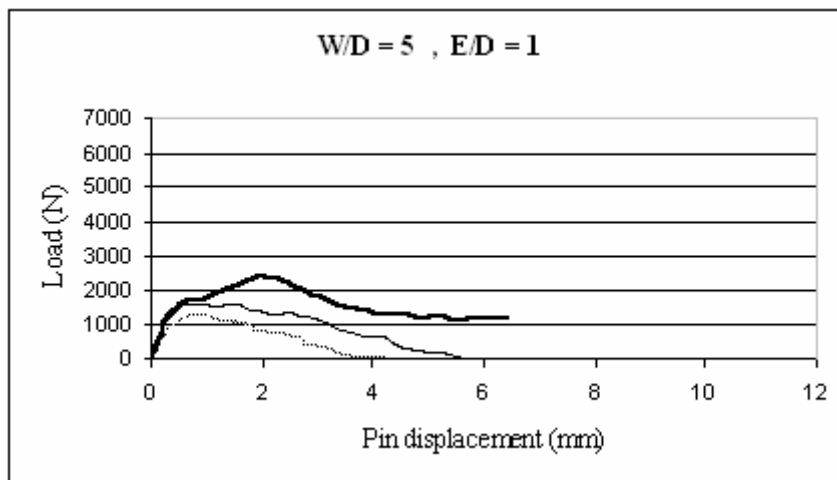
r)
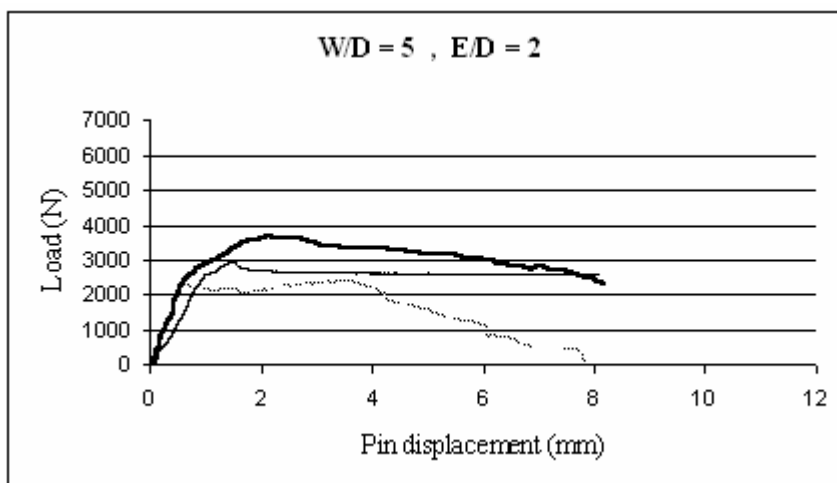
s)
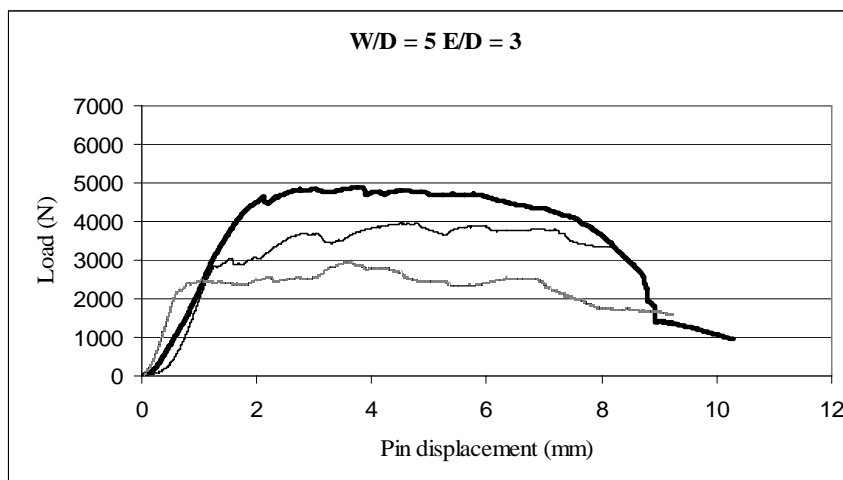
t)
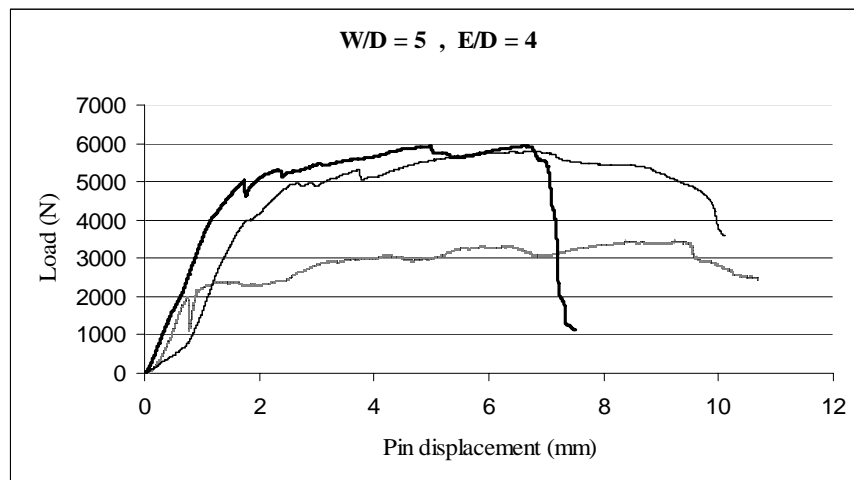
u)
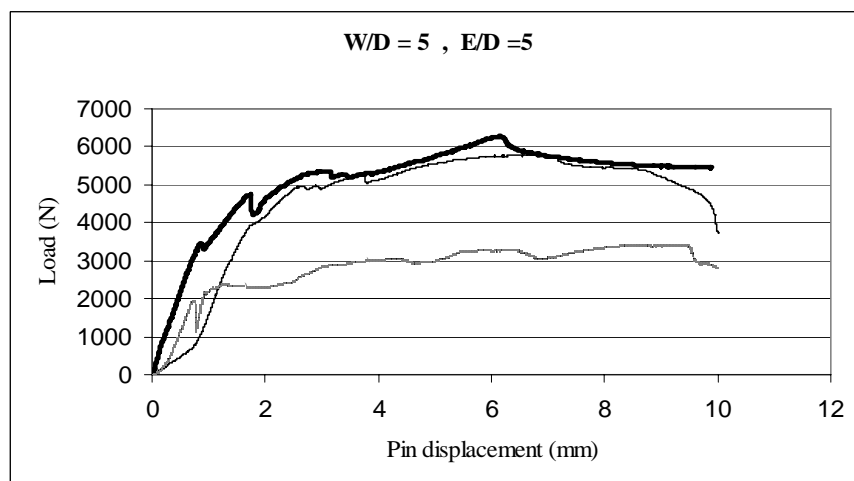
Figure. 7.1. Pin displacement curves.

·············· M = 0 Nm ———— M = 3 Nm ——— M = 6 Nm

a)

E/D = 1

b)

E/D = 2

c)

E/D = 3
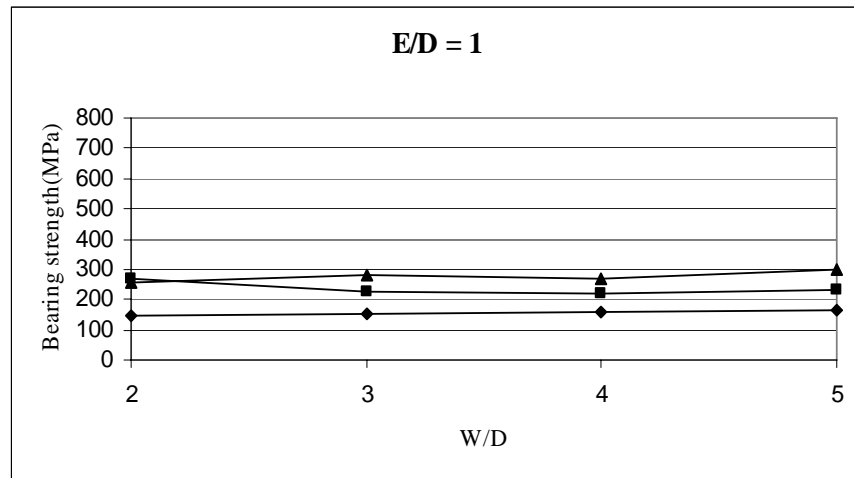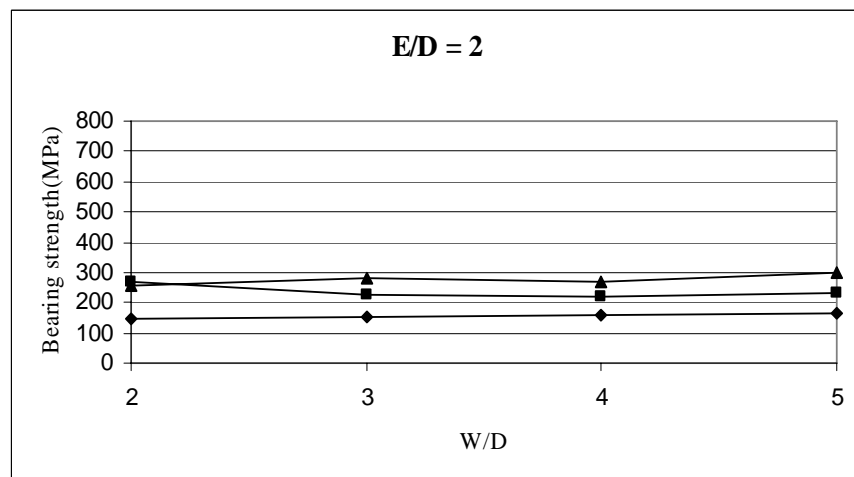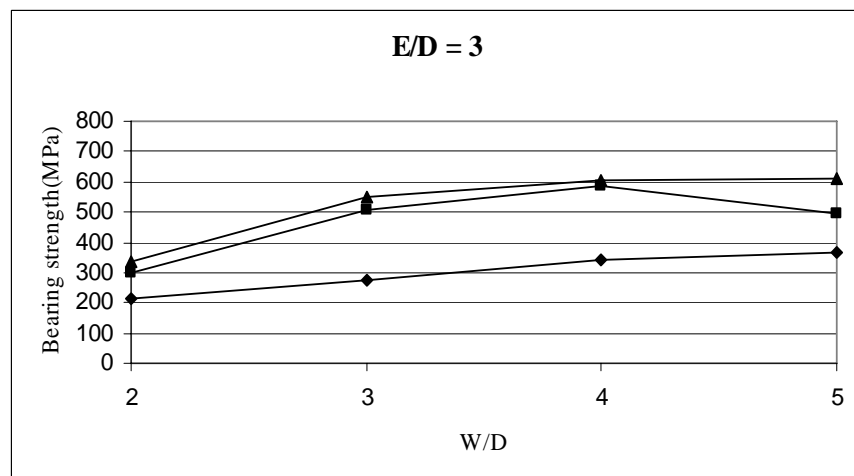
d)
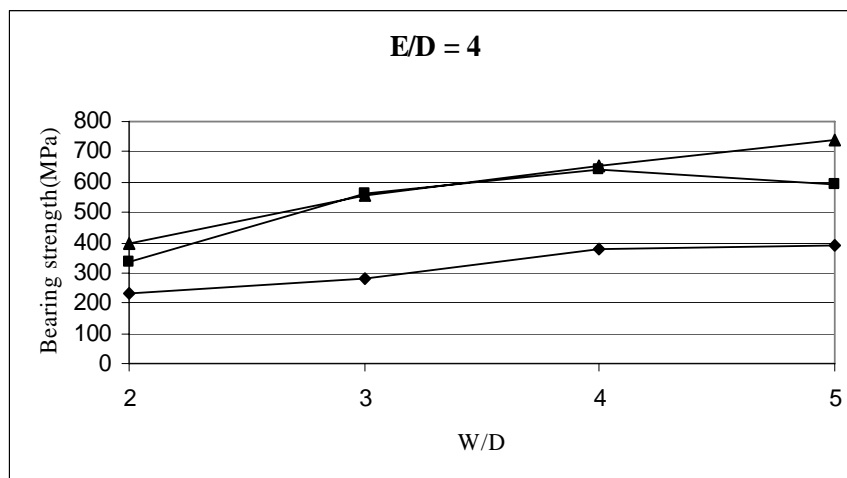
e)
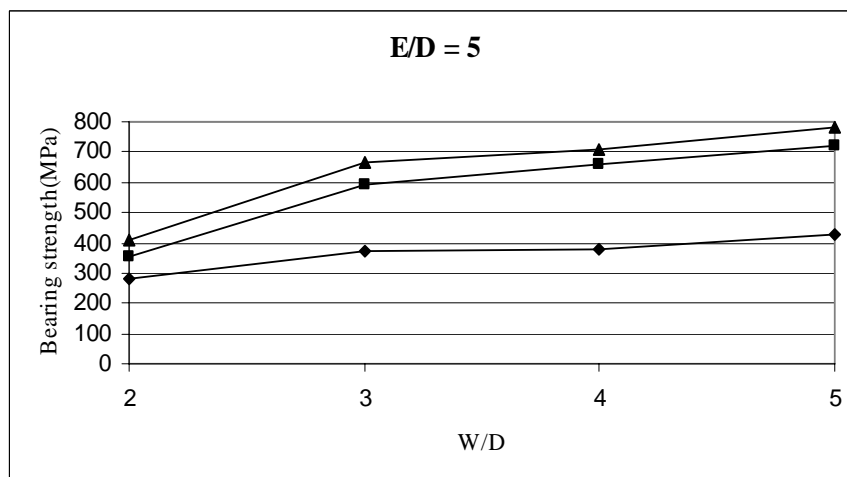
Figure. 7. 2. Effect of W/D on bearing strength.

a)
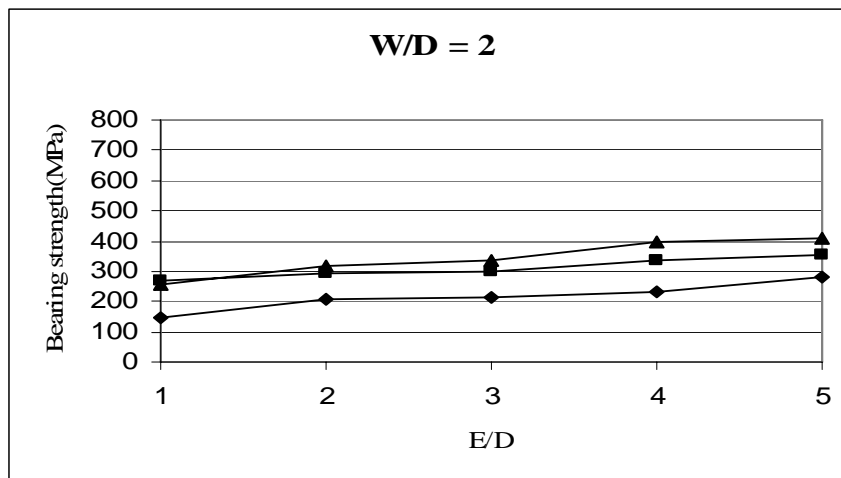
b)
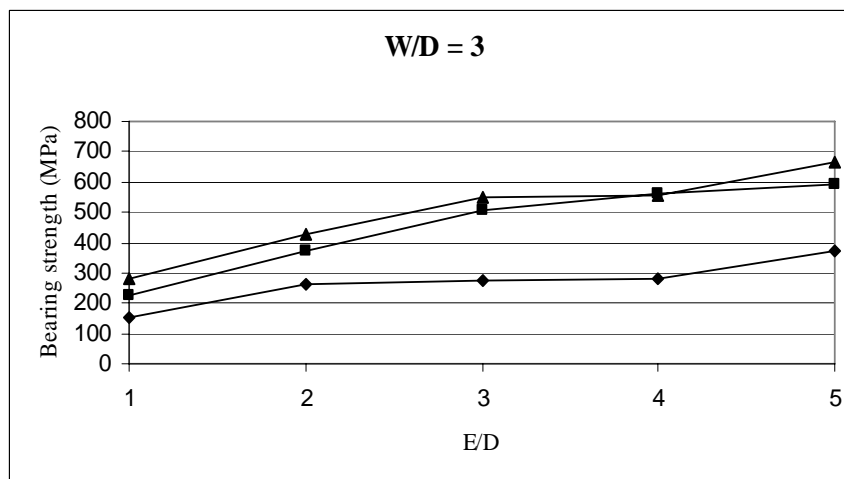
c)
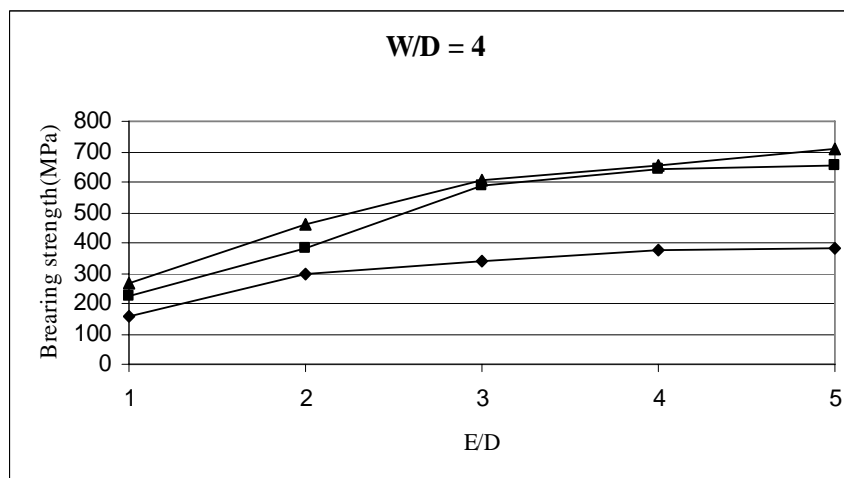
d)
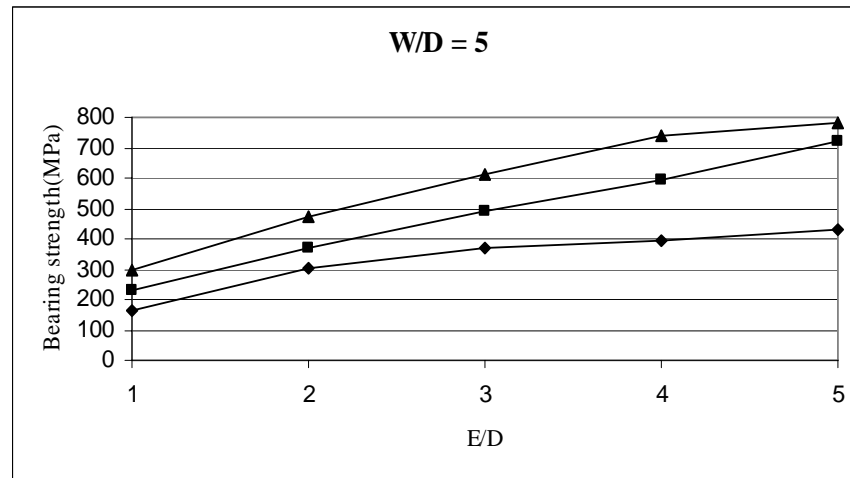
Figure. 7.3. Effect of E/D on bearing strength

7.4 Comparison experimental results with numerical results

In the numerical analysis part studied with LUSAS. 13.6 a satisfying agreement observed only when the failure mode is full bearing mode. In the other modes especially in shear-out mode a great difference between the results is seen. Holding the W/D ratio and preload moment, it is observed that changing of the E/D ratio effects the result in a unimportant value.

During the study of the author, it is observed that a really satisfying agreement between the experimental and numerical results possible with the analyzing of the specimens which has thickness greater than 2 mm. Because of the low thickness of our specimens (t = 1.6 mm) comparison is not gratifying for shear-out, net-tension and combinations of failure modes.

The comparison of the numerical and experimental results is given in Table 7. 2. in addition the analysis for Hashin failure criteria is given in Fig. 7. 4.

Table. 7.1. Failure modes for M = 0 Nm, M = 3 Nm, M = 6 Nm; S : Shear-out, N : Net-tension, B : Bearing.

W/D	E/D	M = 0 Nm	M = 3 Nm	M = 6 Nm
2	1	S	S	S
	2	S	N	N
	3	N	N	N
	4	N	N	N
	5	N	N	N
3	1	S	S	S
	2	B-S	B-N	B-N
	3	B-N	B-N	B-N
	4	B-N	B-N	B-N
	5	B-N	B-N	B-N
4	1	S	S	S
	2	B-S	B	B
	3	B	B-N	B-N
	4	B	B-N	B-N
	5	B	B-N	B-N
5	1	S	S	S
	2	B-S	B	B
	3	B	B	B
	4	B	B	B
	5	B	B	B

Table. 7. 2 . comparison of experimental and numerical results; EXP : Experimental.

W/D	E/D	M = 0 Nm		M = 3 Nm		M = 6 NM	
		EXP.	HASHIN	EXP.	HASHIN	EXP.	HASHIN
2	1	1159 N	1080 N	2142 N	1670 N	2063 N	2640 N
	2	1637 N	1120 N	2329 N	1830 N	2563 N	2645 N
	3	1706 N	1135 N	2410 N	1840 N	2673 N	2670 N
	4	1862 N	1135 N	2703 N	1846 N	3150 N	2672 N
	5	2267 N	1145 N	2839 N	1850 N	3277 N	2810 N
3	1	1223 N	1325 N	1790 N	2437 N	2240 N	3522 N
	2	2124 N	1446 N	2990 N	3021 N	3416 N	3625 N
	3	2200 N	1446 N	4031 N	3320 N	4400 N	3640 N
	4	2260 N	1470 N	4516 N	3575 N	4450 N	3650 N
	5	2994 N	1490 N	4763 N	3590 N	5309 N	3670 N
4	1	1246 N	1310 N	1778 N	2625 N	2137 N	3980 N
	2	2359 N	1340 N	3070 N	3120 N	3694 N	4050 N
	3	2724 N	1350 N	4687 N	3455 N	4845 N	4140 N
	4	3024 N	1370 N	5121 N	3590 N	5217 N	4170 N
	5	3029 N	1420 N	5261 N	3640 N	5671 N	5220 N
5	1	1313 N	1681 N	1840 N	2700 N	2400 N	4830 N
	2	2436 N	1700 N	2950 N	3110 N	3760 N	5020 N
	3	2956 N	1720 N	3951 N	3430 N	4893 N	5212 N
	4	3131 N	1800 N	4764 N	3610 N	5929 N	5275 N
	5	3439 N	1825 N	5784 N	3830 N	6279 N	5312 N

a)

LOAD CASE   =   4
Increment 4 Load Factor = 1.83000
RESULTS FILE =   1
Layer LAYER
MID STRESS
RESULTS ANGLE = MATERIAL
CONTOURS OF HshFbr

	0
	0,0666667
	0,133333
	0,2
	0,266667
	0,333333
	0,4
	0,466667
	0,533333
	0,6
	0,666667
	0,733333
	0,8
	0,866667
	0,933333
	1

Max 1.125 at Node 11
Min 0.5889E-08 at Node 3838
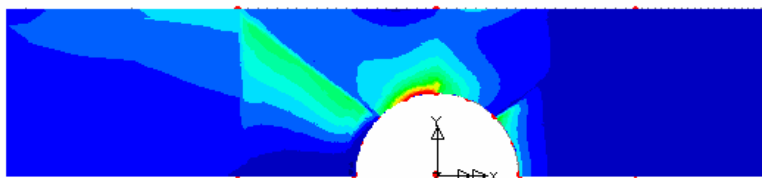
b)

LOAD CASE   =   5
Increment 5 Load Factor = 2.6709
RESULTS FILE =   1
Layer LAYER
MID STRESS
RESULTS ANGLE = MATERIAL
CONTOURS OF HshFbr

	0
	0,0666667
	0,133333
	0,2
	0,266667
	0,333333
	0,4
	0,466667
	0,533333
	0,6
	0,666667
	0,733333
	0,8
	0,866667
	0,933333
	1

Max 0.8015 at Node 1898
Min 0.2826E-07 at Node 3812
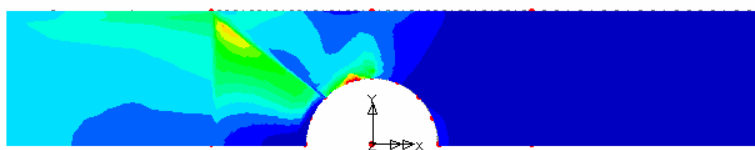
c)

LOAD CASE   =   6
Increment 1 Load Factor = 3.6400
RESULTS FILE =   1
Layer LAYER
MID STRESS
RESULTS ANGLE = MATERIAL
CONTOURS OF HshFbr

0
0,0666667
0,133333
0,2
0,266667
0,333333
0,4
0,466667
0,533333
0,6
0,666667
0,733333
0,8
0,866667
0,933333
1

Max 0.5992 at Node 6006
Min 0.7541E-08 at Node 6743
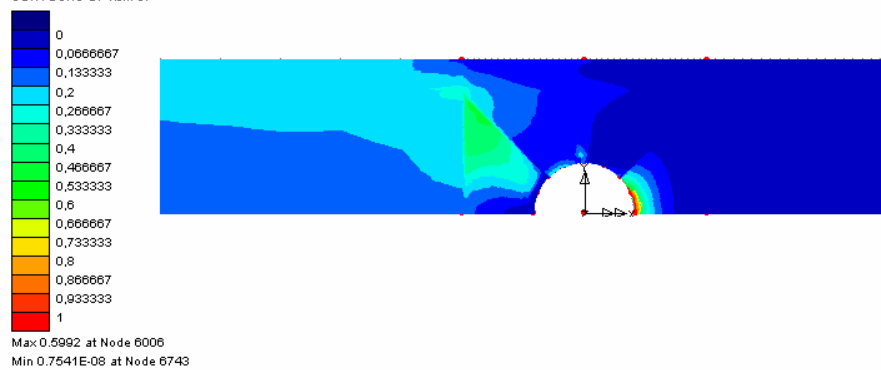
d)

LOAD CASE   =   7
Increment 2 Load Factor = 3.5750
RESULTS FILE =   1
Layer LAYER
MID STRESS
RESULTS ANGLE = MATERIAL
CONTOURS OF HshFbr

0
0,0666667
0,133333
0,2
0,266667
0,333333
0,4
0,466667
0,533333
0,6
0,666667
0,733333
0,8
0,866667
0,933333
1

Max 0.9987 at Node 5316
Min 0.1766E-08 at Node 22
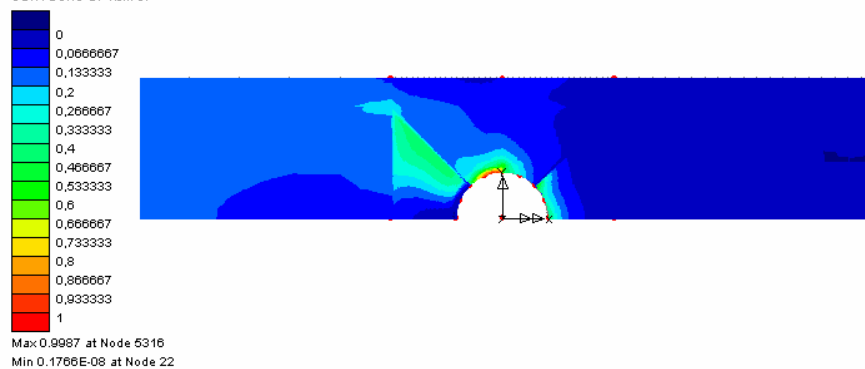
e)

LOAD CASE = 4
Increment 4 Load Factor = 3.12000
RESULTS FILE = 1
Layer LAYER
MID STRESS
RESULTS ANGLE = MATERIAL
CONTOURS OF HshFbr

0
0,0666667
0,133333
0,2
0,266667
0,333333
0,4
0,466667
0,533333
0,6
0,666667
0,733333
0,8
0,866667
0,933333
1

Max 0.7505 at Node 6007
Min 0.2180E-07 at Node 24
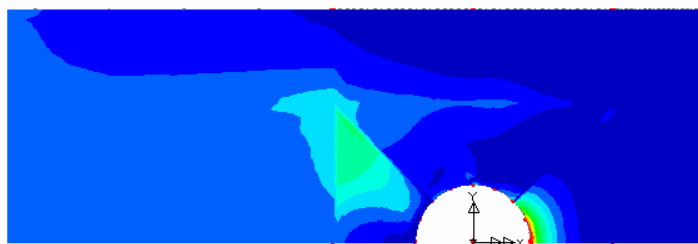
f)

LOAD CASE = 8
Increment 1 Load Factor = 5.2200
RESULTS FILE = 1
Layer LAYER
MID STRESS
RESULTS ANGLE = MATERIAL
CONTOURS OF HshFbr

0
0,0666667
0,133333
0,2
0,266667
0,333333
0,4
0,466667
0,533333
0,6
0,666667
0,733333
0,8
0,866667
0,933333
1

Max 0.7274 at Node 6006
Min 0.2142E-08 at Node 6750
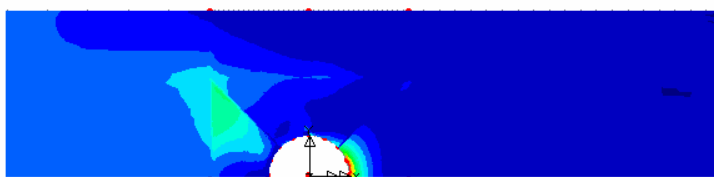
g)

h)
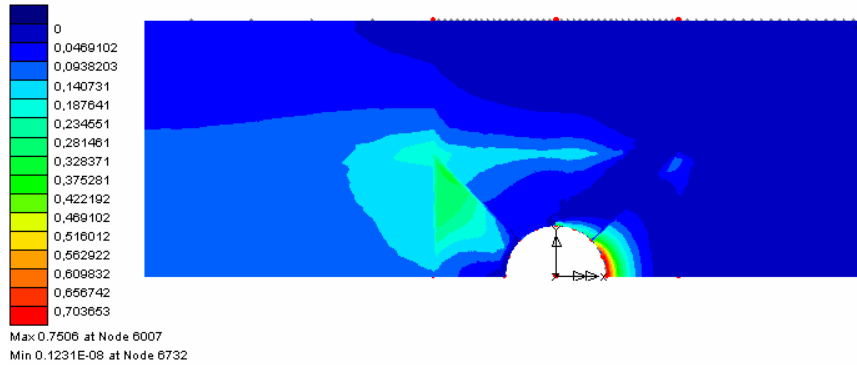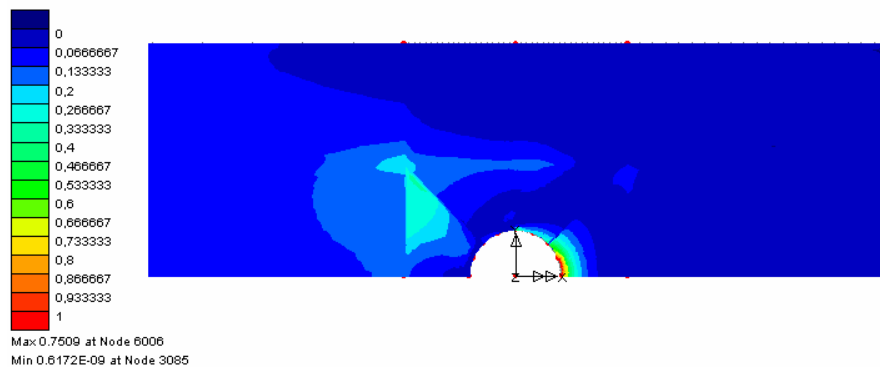
Figure. 7. 4. Analysis for Hashin failure criteria with LUSAS 13.6; a : W/D = 2, E/D = 2, M = 3 Nm, b : W/D = 2, E/D = 3, M = 6 Nm, c : W/D = 3, E/D = 3, M = 6 Nm, d : W/D =3, E/D = 4, M = 3 Nm, e : W/D = 4, E/D = 2, M = 3 Nm, f : W/D =4, E/D = 5, M = 6 Nm, g : W/D = 5, E/D = 3,M = 3 Nm h : W/D = 5, E/D = 4, M = 6 Nm

In these Figures the number in front of the increment load factor is the multiple of the applied load.

The photographs of some specimens after the experimental study is given in Fig. 7. 5. - 7. 6.- 7. 7.-7.8.
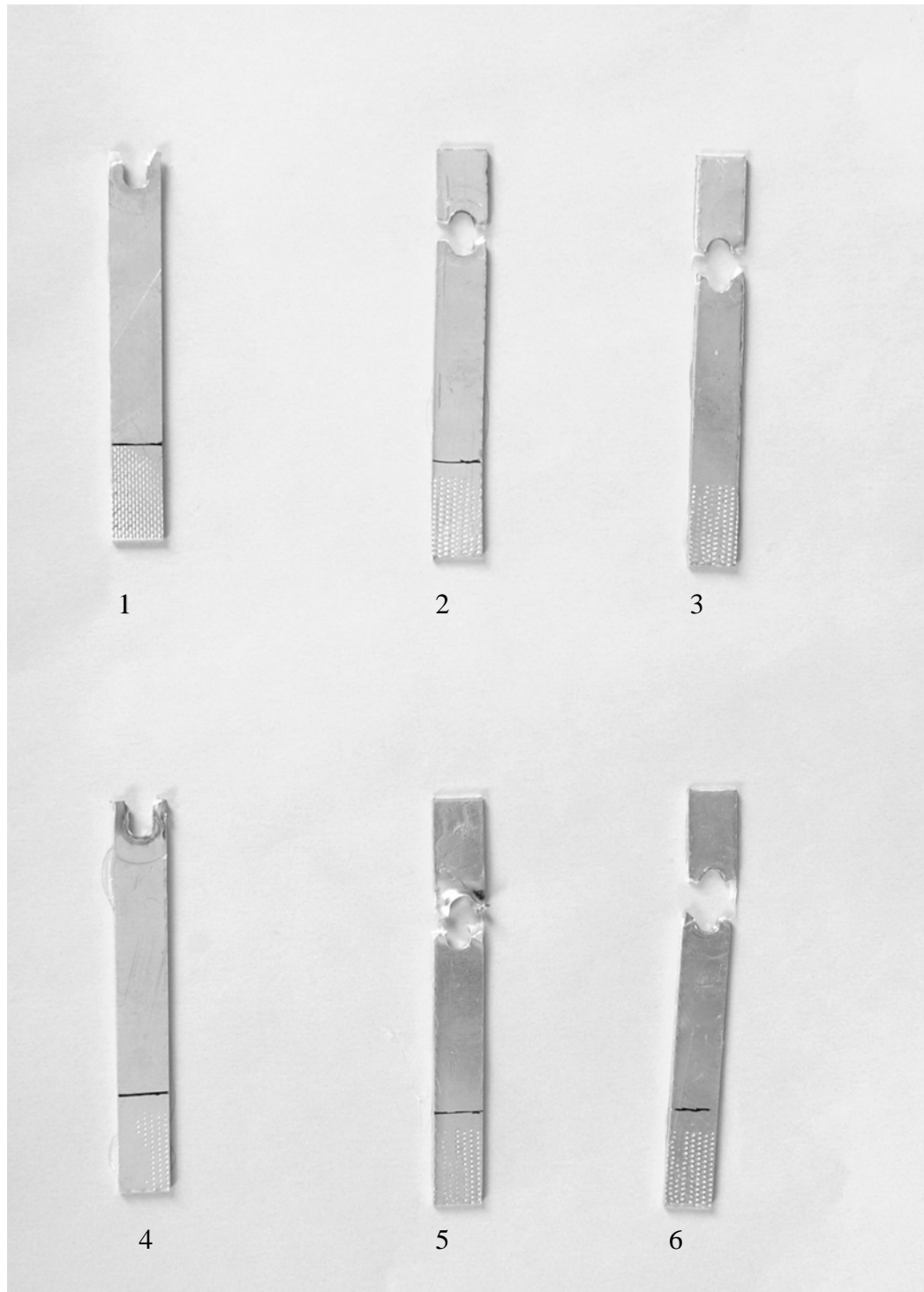
Figure. 7.5. Appearance of changing of preload moments and E/D ratios on specimens where W/D = 2

1: E/D = 1, M = 6 Nm; 2: E/D = 3, M = 3 Nm; 3: E/D = 4, M = 3 Nm; 4: E/D = 2, M = 0 Nm

5 : E/D = 5, M = 0 Nm.
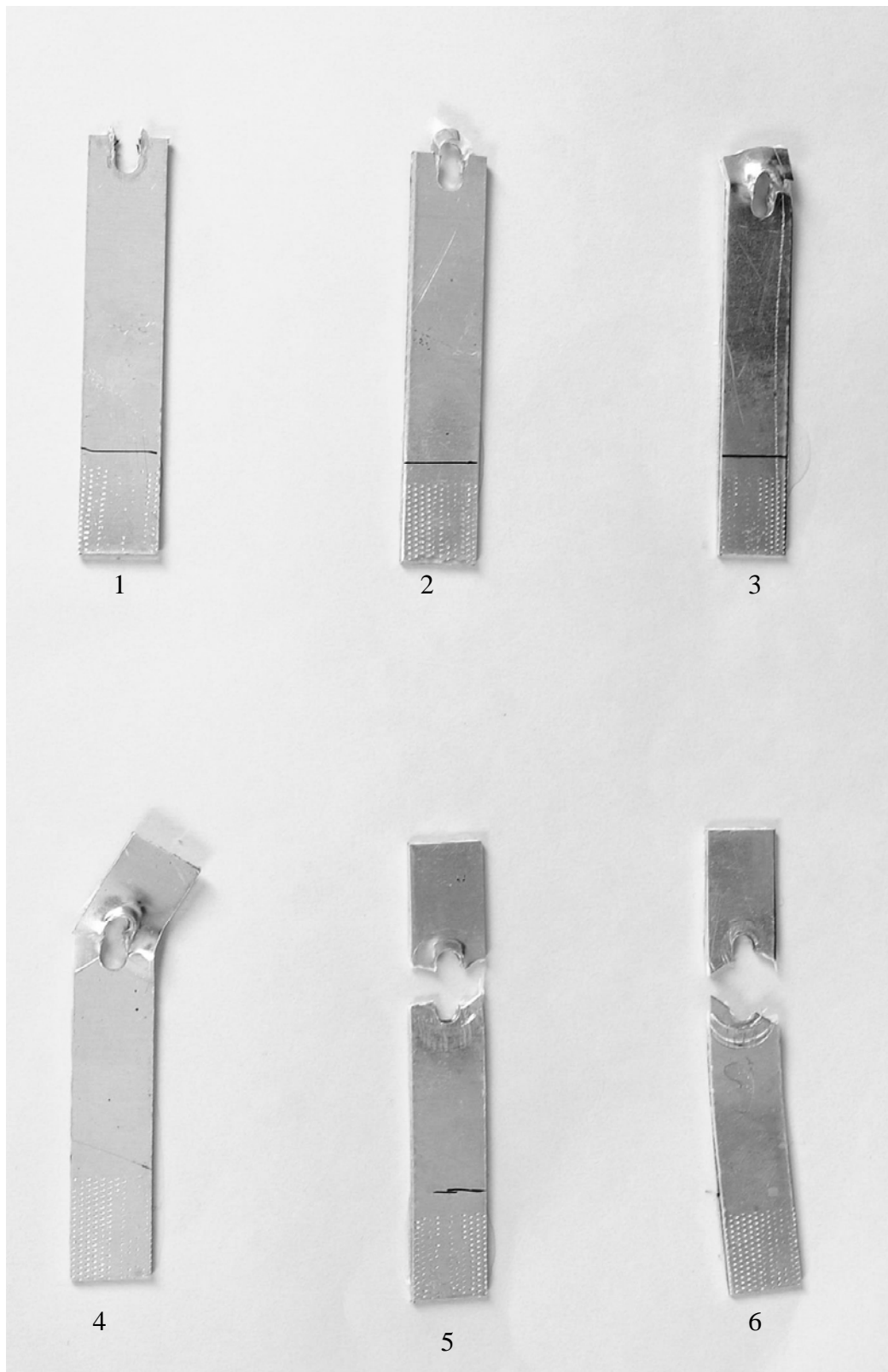
Figure. 7.6. Appearance of changing of preload moments and E/D ratios on specimens where W/D = 3; 1: E/D = 1, M = 3 Nm; 2: E/D = 1, M = 0 Nm; 3: E/D = 2, M = 2 Nm; 4: E/D = 4, M = 0 NM 5: E/D = 5, M = 3 Nm; 6: E/D = 5, M = 6 Nm.
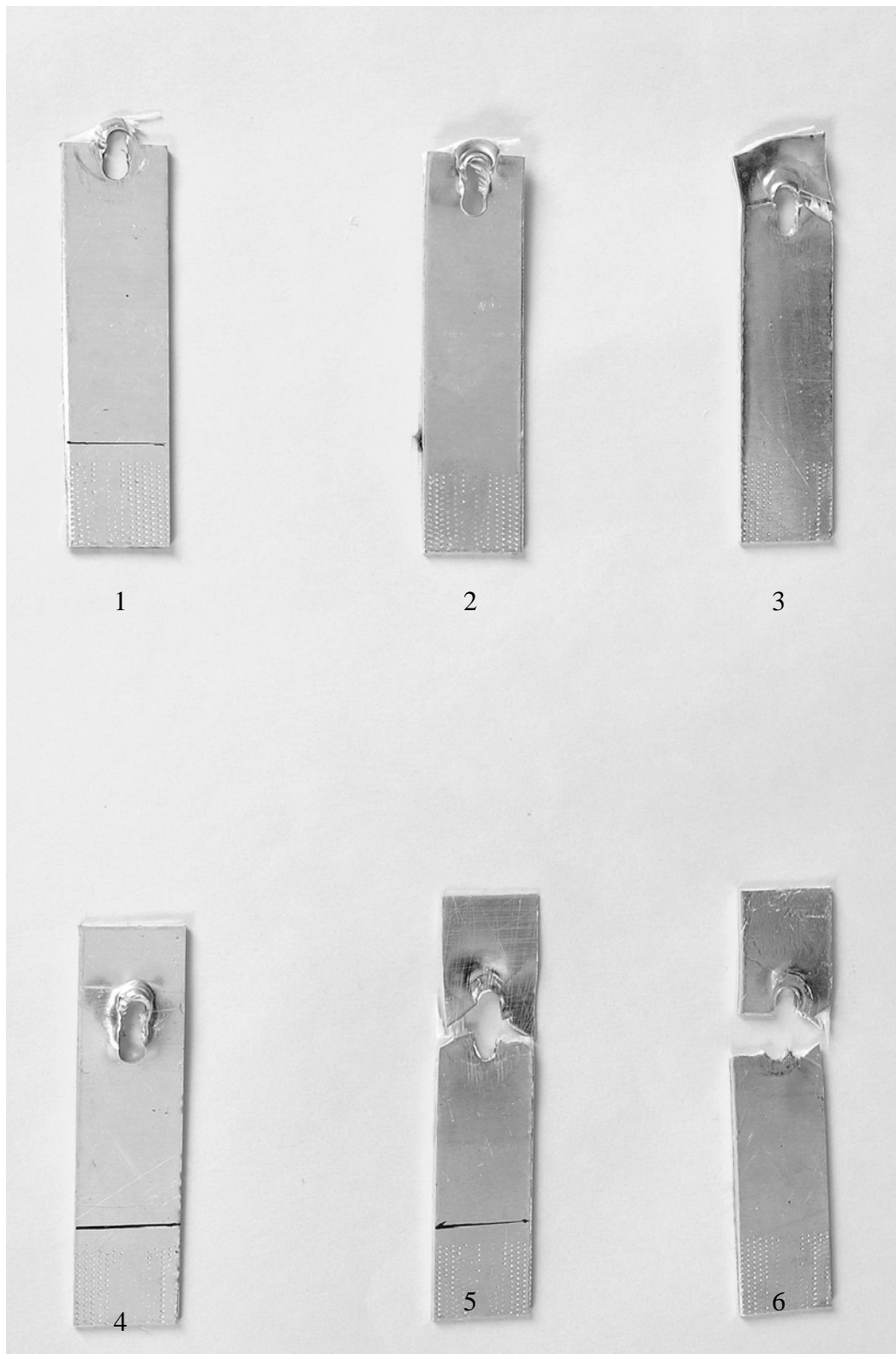
Figure. 7.7. Appearance of changing of preload moments and E/D ratios on specimens where W/D = 4; 1: E/D = 1, M = 6 Nm, 2: E/D = 2, M = 0 Nm; 3: E/D = 3, M = 6 Nm; 4: E/D = 5, M = 3 Nm 5: E/D = 5, M = 3 Nm; 6: E/D = 5, M = 6 Nm
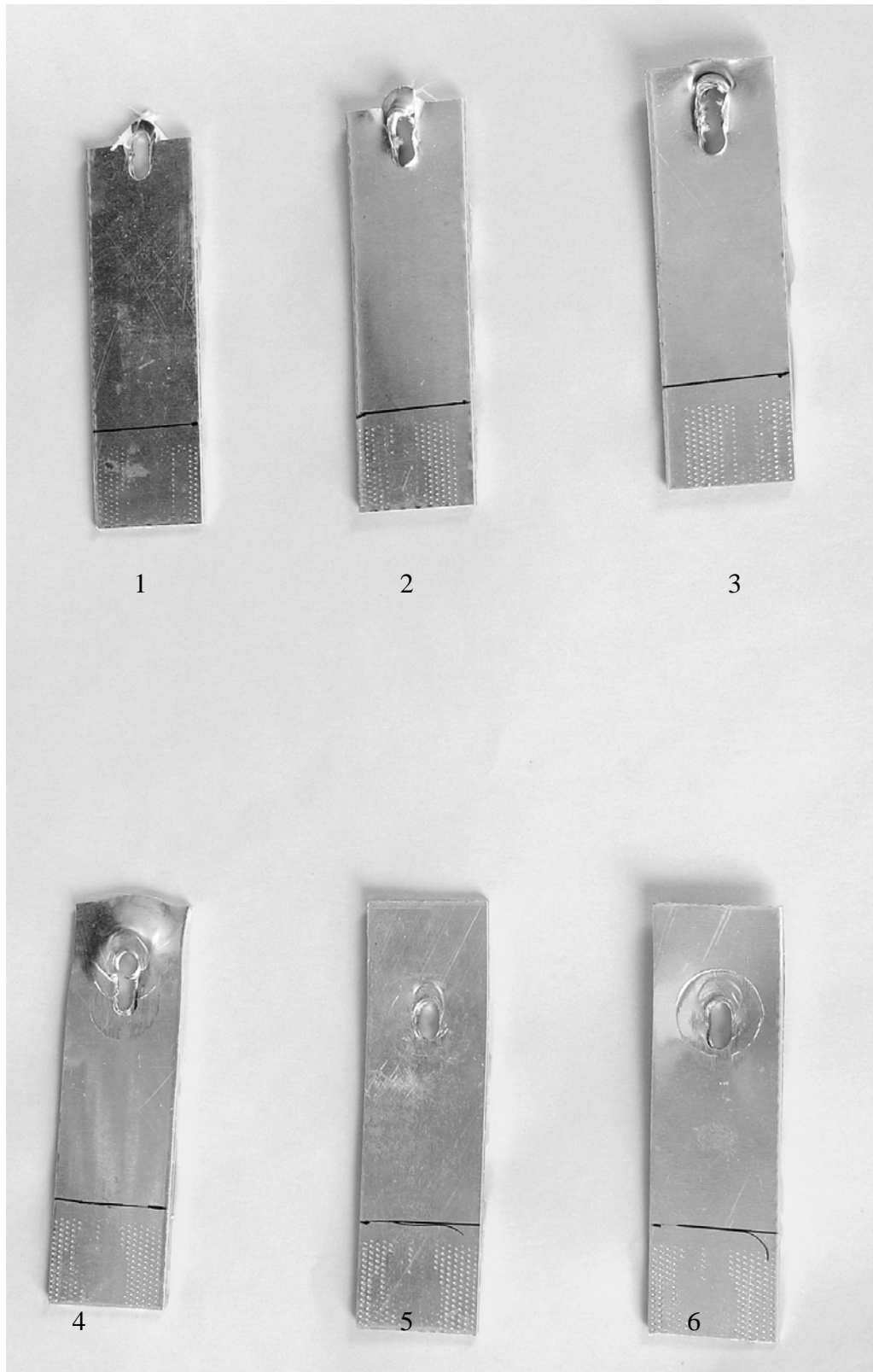
Figure. 7.8.Appearance of changing of preload moments and E/D ratios on specimens where W/D = 5 1: E/D = 1, M = 0 Nm; 2: E/D = 2, M = 0 Nm; 3: E/D = 3, M = 0 Nm; 4: E/D = 4, M = 3 Nm 5: E/D = 5, M = 3 Nm; 6: E/D = 5, M = 6 Nm

CHAPTER EIGHT
CONCLUSION

In the present study, an experimental investigation is carried out on finding bearing strength and failure mode of bolted aluminum-woven glass-epoxy sandwich plate under preload moment. The preload moment is chosen as M = 0 Nm, M = 3 Nm and M = 6 Nm. In order to obtain full bearing strength one of the parameters is changed while the others are held constant.

Basing on experimental results, the following conclusions presented :

1. With increasing of W/D, E/D and M the bearing strength increases.

2. At E/D = 1 the failure mode is always shear-out for all parameters.

3. W/D = 2 is the weakest mode of the sandwich composite plate. And for W/D = 2 , E/D > 1 the net-tension occurs for all the preload moments.

4. At W/D = 5 and E/D > 2 full bearing strength occurs for all the preload moments.

5. Numerical analysis studied by using LUSAS 13.6 gives satisfying results only when the failure mode is full bearing mode and numerical study is not useful for the shear-out failure mode because of the specimen's thickness.

REFERENCES

Aktas, A. & Karakuzu, R. (1999). Failure Analysis of Two-Dimensional Carbon-Epoxy Composite Plate Pinned Joint. *Mechanics of Composite Materials and Structures*, 6, 347-361.

Camanho, P.P. & Matthews, F. L. (1997). Stress analysis and strength prediction of mechanically fastened joints in FRP: a review. *Composites Part A*, 28A, 529-47.

Camanho, P.P. & Matthews, F .L. (1999). A Progressive Damage Model for Mechanically Fastened Joints in Composite Laminates. *Journal of Composite Materials*, 33, 2248-2280.

Chang, F. K., Scott, R. A. & Springer, G. S. (1984)a. Failure of Composite Laminates Containing Pin Loaded Holes- Method and Solution. *Journal of Composite Materials*, 18, 255-278.

Chang, F. K., Scott, R. A., & Springer, G. S. (1984)b. Failure Strength of Nonlinearly Elastic Composite Laminates Containing a Pin Loaded Hole. *Journal of Composite Materials*, 18, 464-477.

Chen, J.C., Lu, C. K., Chiu, C. H., & Chin, H. (1994). On the influence of weave structure on pin-loaded strength of orthogonal 3D composites. *Composites* , 25 , No: 4, 251-262.

Collings, T. A. (1977, January). The strength of bolted joints in multi-directional CFRP laminates. *Composites*, 43-54.

Daniel, I. M & Ishai, O. : *Engineering Mechanics of Composite Materials*. Oxford University Press. New York Oxford. 1994.

Dano, M.L., Gendron, G., & Piccard, A. (2000). Stress and Failure Analysis of Mechanically Fastened Joints in Composite Laminates. *Composite Structures*, *50*, 287-296.

Evans, C. C.(1972). *Whiskers*. Mills & Boon Limited London.

Gibson R. F. (1994). *Principals of composite material mechanics*. McGraw-Hill.

Godwin, E.W., & Matthews, F. L. (1980). A review of the strength of joints in fibre - reinforced plastics. *Composites*, 155-160.

Hassan, N. K. , Mohamedien, M.A., & Rizkalla, S. H. (1996). Finite element analysis of bolted connections for PFRP composites. *Composites*: Part B, 27B, 339-349.

Icten, B. M., & Karakuzu , R. (2002). Progressive failure analysis of pin loaded carbon-epoxy woven composite plates . *Composite Science and Technology*, 62, 1259-1271.

Icten, B. M., Okutan, B. & Karakuzu, R. (2003). Failure strength of Woven Glass Fiber-epoxy Composites Pinned Joints. *Journal of Composite Materials*, 37, 1337-1351.

Icten, B. M., & Sayman, O. (2003). Failure analysis of pin-loaded aluminium glass-epoxy sandwich composite plates. *Composite Science and Technology*, 63,727-737.

Jones RM. (1999). *Mechanics of composite material*. Philadelphia: Taylor& Francis.

Mahmood, H. D. (1991). *Mechanics of Fibrous Composites*. London. Elsevier applied science.

Matthews, F. L., Wong, C. M., & Chryssafitis, S. (1982). Stress distribution around a single bolt in fiber-reinforced plastic. *Composites*, 316-322.

Mathews, F. L. (1989). Design with advanced composite materials. In L. N. Phillips (Eds.), *Joining of Composites*. London: The Design Council.

Pierron, F. , Cerisier, F. & Lermes, M.G. (2000). A numerical and experimental study of woven composite pin-joints. *Journal of Composite Materials*, 34, No:12, 1028-1053.

Richardson, T. (1987). *Composites : A Design Guide*. Industrial Press Inc., New York.

Staab, G. H. (1992). *Laminar Composites*. Butterworth Heınemann.

Stockdale, J. H., & Matthews, F. L. (1976). The effect of clamping pressure on bolt bearing loads in glass fiber-reinforced plastics. *Composites*, 34-39.

Tong L.(2000). Bearing failure of composite bolted joints with non-uniform bolt-to-washer clearance. *Composite Science and Technology*, 31, 609-615.

Watt, W.& B. V. Perov. (1985). *Handbook of Composites*, Vol. 1: Strong Fibers. Amsterdam : North-Holland.

Xiao Y. & Ishikawa T. (2005). Bearing strength and failure behavior of bolted composite joints. *Composite Science and Technology*, 65, 1022-1031.

Zhang, K. D., & Ueng, C. E. S. (1987). Stresses around a pin-loaded hole in orthotropic plates. *Journal of Composite Materials*, 18, 432-446.